ARMY RESEARCH LABORATORY

Flight Demonstration Results of an Inertial Measurement Unit and Global Positioning System Translator Telemetry System

Bradford S. Davis
John A. Condon
T. Gordon Brown

ARL-TR-2630 NOVEMBER 2001

The findings in this report are not to be construed as an official Department of the Army position unless so designated by other authorized documents.

Citation of manufacturer's or trade names does not constitute an official endorsement or approval of the use thereof.

Destroy this report when it is no longer needed. Do not return it to the originator.

ERRATA SHEET

RE: ARL-TR-2630, "Flight Demonstration Results of an Inertial Measurement Unit and Global Positioning System Translator Telemetry System," by Bradford S. Davis et al. of the Weapons and Materials Research Directorate, U.S. Army Research Laboratory

Page 4 of this document should be replaced with the attached page 4.

made 12-V "primary" lithium manganese dioxide battery, manufactured by Ultralife Batteries, powered the entire system. Burke et al. (2000) described the battery development. Power distribution electronics, encoder electronics, and IMU signal-conditioning electronics were designed within three individual printed wiring boards (PWBs) and were assembled between the battery mounting plate and transmitter mounting plate.

2.3 GPS Section

The GPS section was designed and fabricated by APL. It consisted primarily of a custom GPS translator, a COTS GPS antenna pre-amplifier, and a COTS S-band summer. Support electronics included a radio frequency (RF) filter, a COTS power amplifier, and a COTS isolator. APL and NAWC together designed the power regulation PWB within this GPS section. The translator converts the L-band signal from a GPS antenna to an intermediate frequency where it is filtered and combined with a pilot carrier. The composite signal is then converted to S-band and is transmitted to ground.

2.4 Antenna Section

The conical, wrap-around antenna was mounted within the nose of the warhead and shielded by an RF transparent, glass fiber-reinforced plastic radome. A linearly polarized L1/S (receiving/transmitting) dual band antenna from Ball Aerospace was used to obtain the IMU-GPS telemetry data. A rendering of this subassembly is shown in Appendix A, Figure A-3.

3. Mechanical Packaging

3.1 Design and Analysis

ARL's effort entailed mechanically mating the previously developed AMIP telemetry and IMU sections with the GPS section and antenna components. The design intent was to (1) provide modularity of section subassemblies; (2) provide ease of section assembly and disassembly; (3) maintain simple GPS section component layout, mounting, and space efficiency; and (4) provide attachment means to the warhead's main housing and antenna adapter forward bulkhead (AAFB) parts. The assembly drawings detailing the warhead's main housing, AAFB, and internal components are presented in Appendix A.

The GPS section's mounting plate part was designed as a "T" section aluminum 6061 alloy plate whose leg thickness provided allowance for stainless steel machine screw hardware with thread sizes of 4-40 and 18-8 used in its assembly and its attachment to the housing. Its two-piece design provided cost reduction in comparison to a one-piece configuration. The strength of this mounting plate was secondary because of the relatively low operational loads. Aluminum was

Army Research Laboratory
Aberdeen Proving Ground, MD 21005-5066

ARL-TR-2630 November 2001

Flight Demonstration Results of an Inertial Measurement Unit and Global Positioning System Translator Telemetry System

Bradford S. Davis
John A. Condon
T. Gordon Brown
Weapons and Materials Research Directorate

Abstract

The U.S. Army Research Laboratory (ARL) has been evaluating global positioning system (GPS) technology and strap-down inertial measurement units (IMUs) configured from inexpensive, miniature micro-electro-mechanical systems for the purposes of obtaining aerodynamics, trajectory reconstruction, and/or diagnostic information. A GPS translator from the Johns Hopkins University Applied Physics Laboratory and a low-cost IMU designed by ARL from commercial off-the-shelf components were combined with a telemetry system, packaged into a 2.75-inch HYDRA-70 rocket platform, and flight demonstrated. The on-board IMU sensors included accelerometers for measuring the thrust axis and lateral accelerations, angular rate sensors for measuring pitch and yaw rate, a dual axis magnetometer for roll rate and angular yawing motion, and sun-sensing optical sensors to provide a truth measurement for the rate sensor and magnetometer data. Hawk and Weibel tracking radars were also used as a truth measurement of the rocket's velocity and position for comparison to the acquired GPS data and integrated IMU accelerometer data. Results from comparisons of the IMU sensor data to the truth measurements suggest that reasonable aerodynamics and trajectory reconstruction can be achieved. The instrumentation system's development, calibration, demonstration, and the experimental results are described.

ACKNOWLEDGMENTS

The authors would like to thank Mr. Dennis Schneider, of the Simulation Training and Instrumentation Command (STRICOM), and Mr. Ronald Collangelo, formerly of STRICOM, for funding this demonstration as part of the Hardened Subminiature Telemetry and Sensor System (HSTSS) program. There were also a number of people who have made this program a success. The authors wish to recognize each of them by name.

Dr. William D'Amico and Mr. Lawrence Burke, formerly of the U.S. Army Research Laboratory (ARL), were integral in getting HSTSS support for this development and flight demonstration. Mr. Fred Brandon, of Dynamic Sciences, Inc. (DSI), is greatly appreciated for his work in modeling the warhead instrumentation package and for providing the preliminary aerodynamic coefficients that were given to Arrow Tech. Mr. Charles Mitchell of DSI is thanked for supporting the IMU calibration and for fabricating the warhead mechanical prototype hardware, environmental vibration experimental fixture, and calibration fixtures used during the shock experimentation and flight simulator experimentation. Mr. David Hepner of ARL is greatly appreciated for providing support during the flight simulator calibration, data acquisition, and solarsonde data reduction phases. Mr. Jonah Faust, formerly of ARL, is thanked for providing telemetry support during the IMU calibration. Mr. Robert Wert of DSI is thanked for assisting with the pulse code modulation (PCM) data collection during calibration. Mr. Wallace Clay of DSI is appreciated for providing PCM data collection and training support. Mr. Edward Bukoski of DSI is thanked for designing the battery used during flight simulator calibration experiments and for supporting those experiments. Mr. Thomas Harkins of ARL is appreciated for providing simulated rocket IMU data that brought great insight into the experimental data. Mr. Barry Hudler of ARL is thanked for measuring the instrumented warhead and rocket physicals at Transonic Range Facility.

Mr. Michael Boehme, of Johns Hopkins University Applied Physics Laboratory (APL), was integral in orchestrating the GPS translator and data reduction effort. APL was responsible for the GPS translator design and fabrication, GPS section layout, and component integration. Mr. Mark Asher and Mr. Lloyd Linstrom of APL reduced the GPS data. Mr. Steven Myers, of the Naval Air Warfare Center, is thanked for designing and fabricating the telemetry section, IMU signal conditioning, and GPS translator power regulation board.

Mr. Alan Hart and Mr. Charles Ramsdell, of Yuma Proving Ground (YPG), Arizona, are thanked for organizing the experimental site instrumentation and data collection efforts. Mr. Frederick Peabody of YPG provided the radar data, and Mr. Dean Weingarten of YPG provided the meteorological data.

INTENTIONALLY LEFT BLANK

Contents

Figures

Tables

INTENTIONALLY LEFT BLANK

FLIGHT DEMONSTRATION RESULTS OF AN INERTIAL MEASUREMENT UNIT AND GLOBAL POSITIONING SYSTEM TRANSLATOR TELEMETRY SYSTEM

1. Introduction

Obtaining in-flight information for munitions instrumented with "sun-sensing" optical measurement devices and telemetry (TM) packages for the purposes of obtaining aerodynamics, trajectory reconstruction, and/or diagnostic information has been routinely performed by the U.S. Army Research Laboratory (ARL) for many years. This has traditionally been accomplished in concert with radar and video coverage measurement techniques. ARL has recently been evaluating global positioning system (GPS) technology and inertial measurement units (IMUs) configured from inexpensive miniature micro-electro-mechanical systems (MEMS) as a natural replacement or extension of the radar data for supporting operational experiments and evaluations of munitions. To evaluate the concept, the authors demonstrated a GPS translator and a low-cost IMU that had been combined with a telemetry system; these items were packaged into a 2.75-inch HYDRA[1]-70 rocket platform. The demonstration was funded by the Program Director of the Hardened Subminiature Telemetry and Sensor System Program (HSTSS) and was based partially on a study performed by Minor and Rowe (1998) for the HSTSS program.

The objective of the HSTSS HYDRA-70 IMU-GPS-TM Program was to demonstrate the capabilities of acquiring and telemetering the "real time" GPS position and velocity measurements along with the flight dynamics from the IMU from launch through impact. The rocket's conventional warhead section was replaced with an inert instrumentation system and connected to a standard MK66, mod 3 rocket motor (see Figure 1). The GPS and IMU data were downlinked to a ground receiving station via an analog S-band transmitter. The on-board IMU sensors included accelerometers for measuring the thrust axis and lateral accelerations, angular rate sensors for measuring pitch and yaw rate, and a dual axis magnetometer for roll rate and angular yawing motion. ARL's patented solar likeness indicating transducers (SLIT) and associated solarsonde processing (previously known as a yawsonde) provided a truth measurement for the rate sensor and magnetometer data (Hepner, Hollis, & Mitchell 1998). Hawk and Weibel tracking radars were also used to measure the rocket's position and velocity for comparison to the GPS-derived position and IMU-derived velocity data. This report describes the instrumentation system's design, its development, its demonstration, and the flight demonstration results.

[1]Not an acronym

Figure 1. MK66 Rocket Motor With Instrumented Warhead Section.

2. GPS-IMU Instrumentation System

Two warhead instrumentation systems were assembled from parts designed and fabricated by the John Hopkins University Applied Physics Laboratory (APL), ARL, and the Naval Air Warfare Center (NAWC). Figure 2 shows the instrumented warhead system encased inside a custom-designed aluminum housing. The contents of the instrumentation systems were an IMU section, a TM section, a GPS section, and an antenna section (see Appendix A for detailed drawings of the instrumentation system).

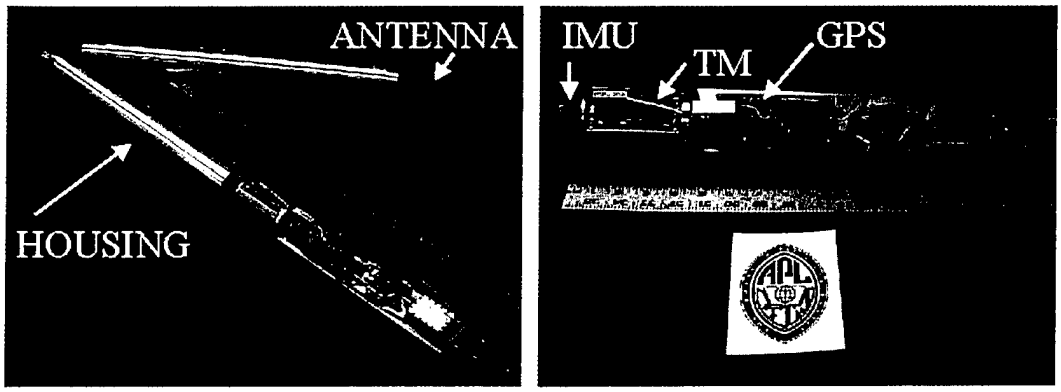

Figure 2. Fully Assembled Instrumented Warhead Section and Its Contents.

2.1 IMU Section

ARL had previously designed the three-axis IMU with low-cost commercial off-the-shelf (COTS) parts during the Advanced Missile Instrumentation Program (AMIP) for the Department of Defense program office for Advanced Threat Infrared Countermeasures, as reported by Condon (1999). Davis, Brown, Condon, Hepner, and Myers (1999) further described the IMU development, calibration, and flight results. For AMIP, it was requested that a warhead replacement telemetry kit be designed, built, and flight tested. This was accomplished during a joint effort among NAWC (China Lake, California), Redstone Technical Test Center (Redstone Arsenal, Alabama), and ARL. The

accelerometers measured both the radial and axial body-fixed accelerations. Magnetometers measured the aspect angle and roll rate relative to the earth's magnetic field. Measurements of the projectile's aspect angle and roll rate with respect to the solar vector, which were made with an optical sensor system (solarsonde), were used as truth metrics for the other body-fixed sensor systems.

The following COTS MEMS accelerometers, magnetometers, and rate sensors were selected for the IMU sensor suite: Analog Devices ADXL190 (one axis, axial acceleration [termed launch accelerometer], ±100-g range), Analog Devices ADXL150 (one axis, axial acceleration [termed longitudinal accelerometer], ±50-g range), Analog Devices ADXL250 (two axes, radial accelerations [termed vertical and horizontal accelerometers], ±50-g range), Honeywell HMC1002 (two axes, roll/attitude axes [termed axial and radial magnetometers], ±2 gauss- (G) range), and Applied Technology Associates angular rate sensor model number 4 (ARS-04) (pitch/yaw axes, ±300°/s range). These sensors have proved to be extremely rugged during high-g survivability experimentation performed by Davis, Brown, Myers, and Hollis (1998) and by Brown and Davis (1999). A thermistor was also included to allow for temperature compensation of the data during the post-processing. The thermistor was embedded within the IMU section and provided temperature to an accuracy of 1° C. A stand-alone signal-conditioning board was used to control the gains, offsets, and low-pass filtering. ARL engineers forwarded the sensitivity and bandwidth specifications to NAWC engineers who designed the circuit wiring diagrams. Gains were controlled so that the full-scale range of each sensor was spread over a 5-V output range. The sensor output at rest was set to the center of the full-scale range—a nominal 2.5 V.

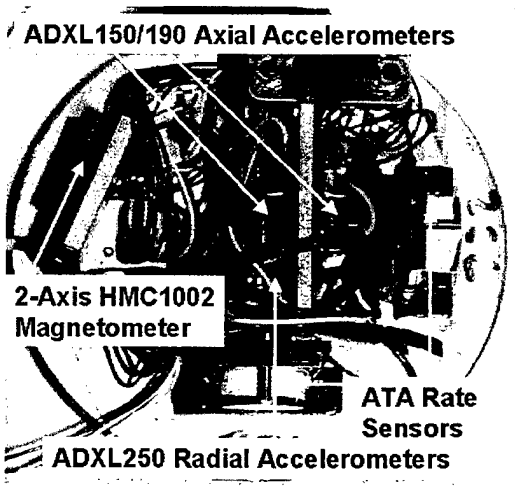

Figure 3. ARL-designed IMU.

2.2 Telemetry Section

This section was designed by NAWC during AMIP. Components of the telemetry system included an S-band transmitter with a frequency of 2213.5 MHz ±500 kHz deviation at 700 mW and 2279.91 MHz ±10 Mhz at 100 mW. A custom-

Ultralife Batteries, powered the entire system. Burke et al. (2000) described the battery development. Power distribution electronics, encoder electronics, and IMU signal-conditioning electronics were designed within three individual printed wiring boards (PWBs) and were assembled between the battery mounting plate and transmitter mounting plate.

2.3 GPS Section

The GPS section was designed and fabricated by APL. It consisted primarily of a custom GPS translator, a COTS GPS antenna pre-amplifier, and a COTS S-band summer. Support electronics included a radio frequency (RF) filter, a COTS power amplifier, and a COTS isolator. APL and NAWC together designed the power regulation PWB within this GPS section. The translator converts the L-band signal from a GPS antenna to an intermediate frequency where it is filtered and combined with a pilot carrier. The composite signal is then converted to S-band and is transmitted to ground.

2.4 Antenna Section

The conical, wrap-around antenna was mounted within the nose of the warhead and shielded by an RF transparent, glass fiber-reinforced plastic radome. A linearly polarized L1/S (receiving/transmitting) dual band antenna from Ball Aerospace was used to obtain the IMU-GPS telemetry data. A rendering of this subassembly is shown in Appendix A, Figure A-3.

3. Mechanical Packaging

3.1 Design and Analysis

ARL's effort entailed mechanically mating the previously developed AMIP telemetry and IMU sections with the GPS section and antenna components. The design intent was to (1) provide modularity of section subassemblies; (2) provide ease of section assembly and disassembly; (3) maintain simple GPS section component layout, mounting, and space efficiency; and (4) provide attachment means to the warhead's main housing and antenna adapter forward bulkhead (AAFB) parts. The assembly drawings detailing the warhead's main housing, AAFB, and internal components are presented in Appendix A.

The GPS section's mounting plate part was designed as a "T" section aluminum 6061 alloy plate whose leg thickness provided allowance for stainless steel machine screw hardware with thread sizes of 4-40 and 18-8 used in its assembly and its attachment to the housing. Its two-piece design provided cost reduction in comparison to a one-piece configuration. The strength of this mounting plate was secondary because of the relatively low operational loads. Aluminum was

the material of choice for this part because of its good heat conduction and adequate strength properties. Design stress calculations for screw hardware were made to ensure their structural integrity under operational loadings of launch setback and rocket motor-induced axial acceleration and spin. Inertia-induced shear loadings were statically applied to the screws that connected the mounting plate with the TM section to the housing. These shear loadings were also applied to the screws that held the GPS section components to this mounting plate.

The AAFB part provided a mounting for the antenna and attachment to the housing. It also provided for mounting of the four SLIT sensors, a pull-away external power change-over connector, and the antenna radome (see Appendix A, Figure A-3). The power change-over feature provided for system power before launch and for subsequent switching to internal battery power upon connector detachment during launch. Design stress calculations for the 4-40, 18-8 stainless steel housing attachment screws were made to ensure structural integrity under operational loadings of launch setback and rocket motor-induced torque.

The aluminum 6061 alloy housing was designed to extend the AAFB and its attached antenna and solarsonde sensors past the end of the metal rocket launch tube to facilitate GPS signal acquisition before launch. Computer-aided engineering (CAE)-based structural stress finite element analysis (FEA) was conducted on the housing to ensure its integrity under operational loadings. FEA results of this analysis are shown in Appendix B. The analysis was configured with statically applied loadings, linear material properties, and a two-dimensional, axis-symmetrical modeling scheme. The housing's design required an outer diameter of 2.75 inches and an inner diameter of 2.5 inches to allow "pass-through" clearance for the existing TM and IMU sections. The 0.125-inch wall thickness within the instrumentation section of the housing (2.5-in. diameter by 17-in. long bore) provided adequate strength and allowed for an acceptable machining with the use of in-house lathe tooling.

Aeroballistic properties of this custom warhead were not matched to the existing fielded M151 training warhead or M257 illuminating tactical warhead. However, flight stability was verified during the design with an interior ballistic and trajectory simulation software tool entitled "projectile design and analysis system" version 2000 (PRODAS 2000) (see Appendix C). CAE/computer-aided drafting and design (CADD) software was used to mechanically package the warhead, provide interference checking, and to provide shop fabrication drawings. The CAE/CADD tool was also used to generate warhead physical properties including weight, longitudinal (axial) center of gravity (c.g.) estimates, and axial and transverse moments of inertia (Ix, Iy) input data for preliminary PRODAS simulations. Lateral (radial) c.g. offset from the housing's geometric centerline was minimized by designing a steel counterweight that attached to the interior of the housing, following insertion of the IMU-GPS-TM subassembly.

3.2 Integration

Following mechanical part fabrication, two instrumentation systems were assembled, functionally tested, and environmentally tested at APL. Physical properties of the assembled warhead systems were measured at the Transonic Range Facility, Aberdeen Proving Ground, Maryland. The physical properties from a typical MK66, mod3 rocket motor were measured separately. The instrumentation system and rocket motor physical properties were then mathematically combined. This was done because of constraints on the equipment and ease of measurement. Table 1 shows the estimated physical data of each instrumentation system before rocket ignition and after rocket burnout. Warhead physical properties of weight, c.g., Ix, and Iy, as calculated by the CAE/CADD tool and used in the PRODAS 2000 simulations, were as follow: 8.63 lb (3.79 kg), 14.17 in. (0.36 m), 10.94 lb-in^2 (3.2E-03 kg-m^2), and 577.53 lb-in^2 (1.69E-01 kg-m^2), respectively.

Table 1. Instrumented Rocket Physical Data
(English and metric units)

		ARL 1		ARL2	
	Units	Before Ignition	After Burnout	Before Ignition	After Burnout
Weight	pound	22.20	14.98	22.11	14.89
c.g.	in. from base	32.27	37.35	32.39	37.56
Ix	lb-in^2	25.46	18.96	25.33	18.83
Iy	lb-in^2	9005.0	7619.4	8960.4	7615.6
diameter	in.	2.75	2.75	2.75	2.75
length	in.	71.18	71.18	71.18	71.18
calibers	cal	25.88	25.88	25.88	25.88
Weight	kilograms	10.07	6.79	10.03	6.75
c.g.	m from base	0.820	0.949	0.823	0.954
Ix	kg-m^2	7.450E-03	5.549E-03	7.412E-03	5.511E-03
Iy	kg-m^2	2.635	2.229	2.622	2.228
diameter	m`	0.070	0.070	0.070	0.070
length	m	1.808	1.808	1.808	1.808
calibers	cal	25.88	25.88	25.88	25.88

4. Calibration

A series of calibration experiments was required to adequately characterize the on-board IMU sensor suite. The experiments included the determination of scale factor (SF), zero-rate bias, cross-axis sensitivity, misalignment, radial offset, and

noise. All these experiments were performed at ambient temperature conditions with various apparati at ARL. The detailed calibration experimental plan is shown in Table 2. Algorithms developed by ARL provided the capability to archive the pulse code modulation (PCM)-transmitted IMU data into a portable data acquisition system and to separate the individual signals. An Inter-Range Instrumentation Group (IRIG) receiver card and other hardware were required to synchronize the sensor output. The binary archived data were then translated into decimal units by data acquisition software for quick turn-around time display and engineering unit conversion.

Table 2. Calibration Experimental Plan

Sensor Being Studied	Part No.	Calibration Apparati	Experimental Description	Output Variable
Accelerometer	ADXL150 ADXL190 ADXL250	Flight simulator	30 - 0 Hz roll down mounted straight up	Spin bias for all 3 accel
		Level table (0g and ±1-g calibration)	50-g slam mounted up	SF ADXL190,ADXL150
			Point down (up data are in Exp A)	SF ADXL190,ADXL150 & 0-g bias ADXL250
			Roll 360 degrees mounted sideways	SF ADXL250 & 0-g bias ADXL190, ADXL150
Magnetometer	HMC1002	Helmholtz coil	Field = 0 to 0.5 gauss	SF and 0-field bias
		Helmholtz coil	Simulated roll rate = 15, 30, 45 Hz	0-field bias
Rate sensor	ARS-04R		Input rate (deg/s)/spin rate (Hz)/ type of motion	
		Flight simulator	30/10/coning+overturning	SF
			30/20/coning+overturning	SF
			30/30/0spin dwn/con+overt	SF
			60/10/coning+overturning	SF
			60/20/coning+overturning	SF
			60/30/0spin dwn/con+overt	SF
			60/15/coning+overturning	SF
			60/30/coning+overturning	SF
			120/15/coning+overturning	SF
Optical sensor	SLIT	Optical bench	360 degress in roll angle table	Aspect angle look-up
			± 90 degrees in aspect angle	

The first experiment was to calibrate the accelerometers for scale factor, misalignment, and bias. The instrumentation system was placed in a precisely fabricated alignment fixture and subjected to a ±1-g calibration. This is the simplest method used to calibrate the accelerometers but may not be the most accurate. The radial accelerometers were calibrated first. To do this, the warhead

instrumentation system was held in place by bolts at index points marked on its aluminum housing (see Figure 4) and then rotated in 90-degree increments. The axial accelerometers were ±1-g calibrated by placing the instrumentation system on a level table, making a measurement, and repeating after a 180-degree pitch rotation.

Next, the roll and yaw magnetometers were calibrated in a single-axis Helmholtz coil. The coil was attached to a power supply generator that allowed the magnetic field strength at Yuma Proving Ground (YPG), Arizona, to be simulated. Calibrations were performed over a range of field intensity (0.4 to 0.6 gauss [G]) and frequency (0 to 45 Hz) to cover all possible flight scenarios. The alignment fixture was used to orient the roll magnetometer as seen in Figure 5. The IMU within the housing was placed in the center of a single-axis Helmholtz coil to ensure field uniformity. The housings were positioned so that the HM1002 sensor was oriented at its maximum sensitivity to the field. To calibrate the yaw magnetometer, the instrumentation system was placed vertically through the coil. HM1002 output was viewed on a spectrum analyzer to determine maximum amplitude and phase information. Bias, scale factor, and cross-axis sensitivity errors were determined from the measurements.

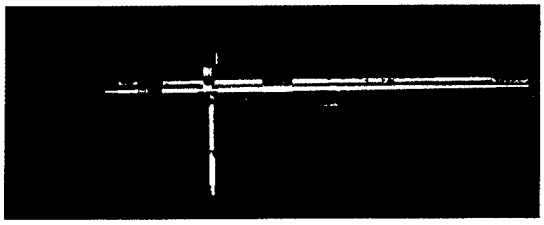

Figure 4. Alignment Calibration Fixture Setup.

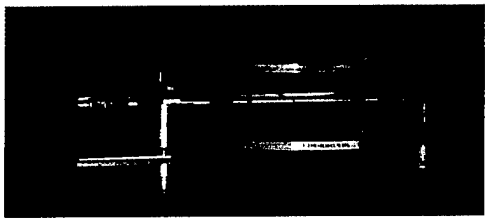

Figure 5. Single-axis Helmholtz Coil Setup.

The instrumentation system was then shock evaluated to 28 g's to verify its survivability during shock and to measure the scale factor of the accelerometers by an alternate method. Figure 6 shows the warhead instrumentation system attached to ARL's IMPAC66 high velocity and acceleration (HVA) shock evaluation machine by a specially designed mounting fixture just before shocking. This machine uses high-pressure gas to raise or lower a drop table on command. Once the table is at the desired height, an elastic cord normally assists in pulling the drop table toward an anvil that is covered with mitigation material for high-g shock simulations. For this set of experiments, the cord was detached, and a piston-like dampening device was installed to create a low-g simulation. Deceleration was measured by a reference accelerometer mounted directly to the drop table. An analog-to-digital (A/D) system comprised of National Instruments hardware and Labview software was used to record the data. Figure 7 shows an example of the response from both axial accelerometers (ADXL190 and 150) as compared to the reference accelerometer. The scale factor

by this method was 10% lower than that obtained from the ±1-g approach. This was because the reference accelerometer, placed directly on the mounting, saw a larger shock than the IMU axial accelerometers did because the shock was mitigated, or its sensitivity was out of calibration. The latter was most likely the case since the scale factor from the ±1g-calibration was used for the flight experimental data, and it more closely matched the radar-derived velocity data.

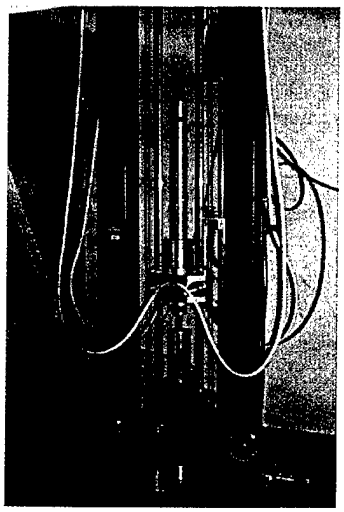

Figure 6. Shock Table Setup.

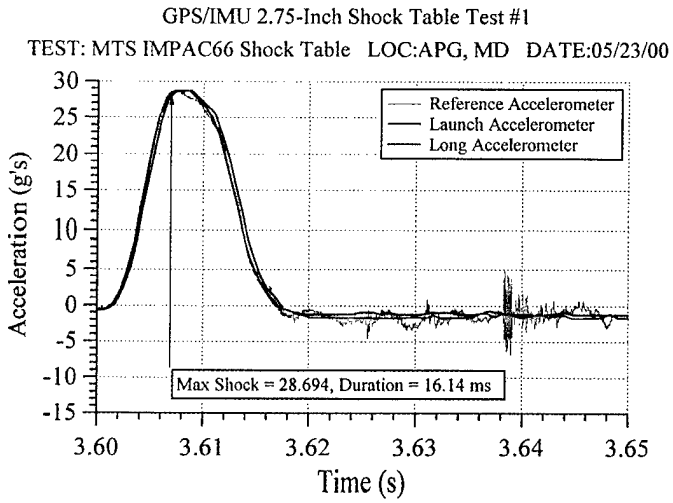

Figure 7. Axial Accelerometer Output During Shock Evaluation.

Finally, the instrumentation system was attached to ARL's 3-degree-of-freedom rate table, flight simulator, manufactured by Carco Electronics. The instrumentation system was mounted to the specially designed fixture, which in turn was mounted to the flight simulator's top bearing, as seen in Figure 8. The fixture contained a specially designed rechargeable battery to power the system externally, eliminating the need to power the unit via a "slip ring." The flight simulator's inner, outer, and roll axes were controlled remotely by a personal computer. Position data from optical encoders were read and compared to input data until the differences between the commanded positions and read positions were within the desired limit.

The flight simulator was programmed to follow various motions used in calibrating the angular rate sensors and accelerometers. A typical motion used in the calibration was a coning motion with a prescribed overturning during rotation. Using the temporal history of the measured flight simulator positions, we calculated an angular rate history and used it as the reference. The angular rate sensor data were compared to this reference. Since the motion was roll modulated, both rate sensors could be calibrated at once. In this manner, scale factors and biases were obtained. The coning motion and spin rate were varied independently in an attempt to decouple the sensitivities and misalignment.

Although the roll rate had some effect on the calibration, only a linear scale factor and bias were used, as determined from the varying amplitude of the coning motion. For the last experiment, the flight simulator was spun to 30 Hz so that the radial accelerometer's offset radius relative to the roll axis could be estimated. A positive or negative sign of the offset radius indicated an inward or outward direction of the accelerometer's sensitive axis. The accelerometer and angular rate sensor calibration data are summarized in Table 3.

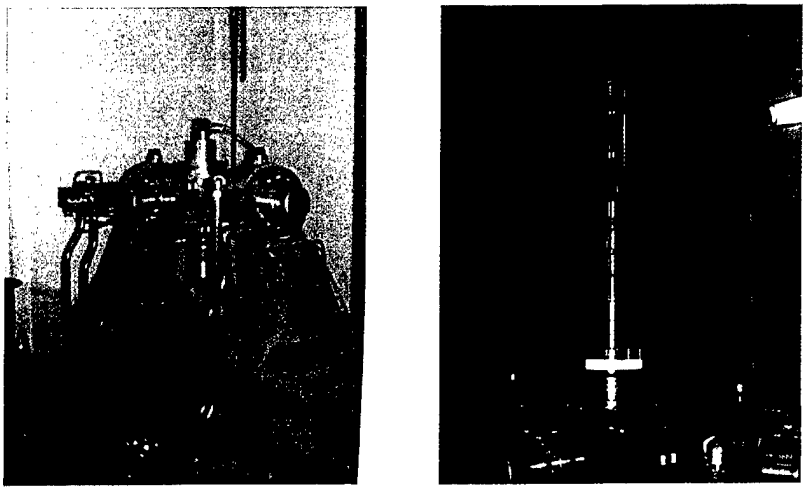

Figure 8. Flight Simulator Setup.

Table 3. Accelerometer and Rate Sensor Calibration Data

Nomenclature (accelerometer)	Orientation	0g bias (bits)	Alignment Fixture Noise SF (bits/g)	Noise SD (bits)	Misalignment X (deg)	Misalignment Y (deg)	Misalignment Z (deg)	Measurement Method Flight Simulator Offset Radius (mm)	Measurement Method CAD Simulation Offset From c.g. (m)	Shock Table SF (bits/g)
Launch (ADXL 190)	Axial	443.69	17.21	1.02	0.25	0.44		0.19	0.1483	15.82
Longitudinal (ADXL150)	Axial	41.22	33.95	1.08	-1.98	-1.53		0.00	0.1483	30.69
Horizontal (ADXL 250x)	Radial	107.90	31.98	0.95		0.29	-0.28	1.23	0.1385	
Vertical (ADXL250y)	Radial	150.16	32.60	0.96	-4.82		0.42	-2.15	0.1385	
(Rate sensor)			(bits/deg/s)							
Pitch rate (ATA ARS-4)	Pitch		0.04							
Yaw rate (ATA ARS-4)	Yaw		0.09							

5. Flight Demonstration Description

The flight demonstration was conducted between September 13 and 14, 2000, at Rocket Alley, YPG (see Table 4). A total of seven rounds (three warmer rounds, two instrumented rounds, and two mock-up rounds) was fired over the 2-day period. The warmer rounds were configured with M151 training warheads and were fired to verify that the tracking radar and time zero instrumentation were fully operational. The mock-up rounds contained no electronics but physically simulated the instrumented warheads enough to be an aero-ballistic match. The mock-up rounds provided qualitative verification of flight characteristics and aided in the spotting of instrumented rounds for their subsequent recovery.

Table 4. Experimental Matrix

YPG Round No.	ARL/APL Round No.	Firing Date	Local Time (hr:min:s)	Projectile Configuration
11	Mock-up	13-Sep-00	17:11:30	MK66, mod3 with mock-up warhead
14	2	13-Sep-00	17:52:54	MK66, mod3 with instrumented warhead
12	Mock-up	14-Sep-00	16:06:53	MK66, mod3 with mock-up warhead
15	1	14-Sep-00	16:36:07	MK66, mod3 with instrumented warhead

A TM van, instrumented with a TM receiving station and data acquisition system, served as the ground station. ARL, NAWC, and APL engineers operated it. The IMU data were acquired with the PCM "lunchbox" computer from Dewetron. Other instrumentation included a Hawk tracking radar, Weibel tracking radar, GPS receiving antenna, meteorological (MET) station, and video coverage. Instrumentation warheads were temperature conditioned to ambient conditions before launch. Just before firing, ARL engineers performed final environmental static calibration of the on-board IMU sensors.

A 19-tube M261 launcher was used to fire the rockets (see Figure 9). The launcher's quadrant elevation was inclined 15 degrees from horizontal, and its azimuth was 340 degrees clockwise from true north. The warhead instrumentation system extended from the launcher so that the GPS and IMU data could be recorded in real time through the telemetry system before firing and throughout the warhead's flight. The absolute time zero and launcher exit time were determined from two infrared (IR) detectors. One IR detector was placed behind the launcher to sense rocket ignition and trigger the radars. The other was placed in front of the launcher to sense when the rocket exited the launcher (see Figure 10).

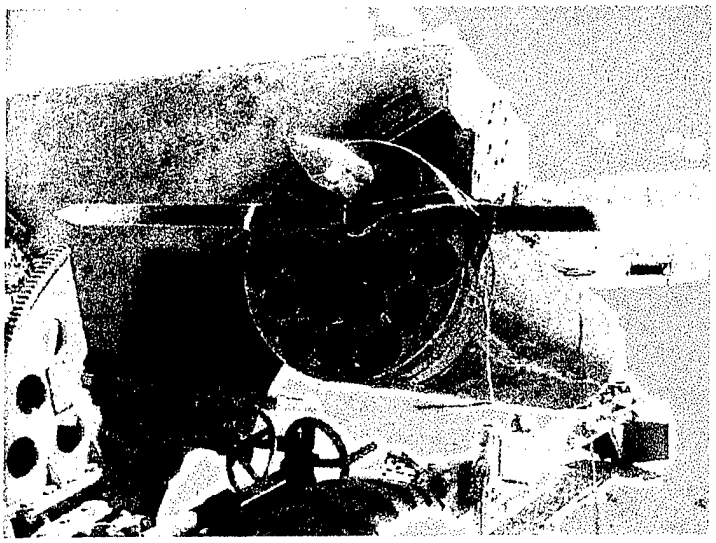

Figure 9. Warhead Orientation Within the M261 Launcher Before Firing.

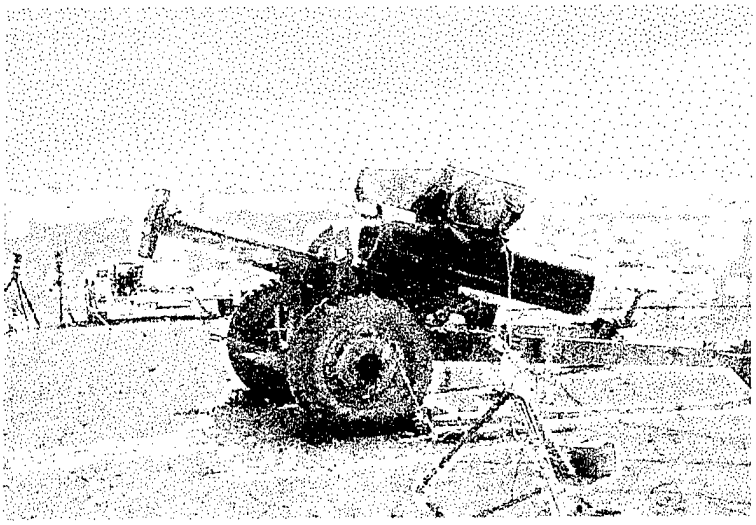

Figure 10. Flight Demonstration Setup Showing the Rear and Forward IR Cameras.

Figure 11 shows select video images of instrumented rocket ARL 1/YPG 15 leaving the launch tube with a clear visual indication of launcher exit. The traces from the IR detectors were plotted along with IRIG time and telemetry automatic gain control (AGC) (a measure of the receiver's signal strength) to synchronize all the data (see Figure 12). Table 5 shows some of the resulting experimental measurements obtained from the IR detectors and radars. When the IRIG time from the rear IR detector was used as the absolute time, there was a 6.94-ms discrepancy between when the ignition of the rocket was first observed by the rear IR and when the longitudinal accelerometer and other IMU sensors experienced first motion. To synchronize the data, the IMU data were shifted by 6.94 ms so that first motion and absolute time zero happened simultaneously.

The authors could not determine exactly why this discrepancy existed, but it is possible the independent telemetry station and range IRIG cards were not fully synchronized.

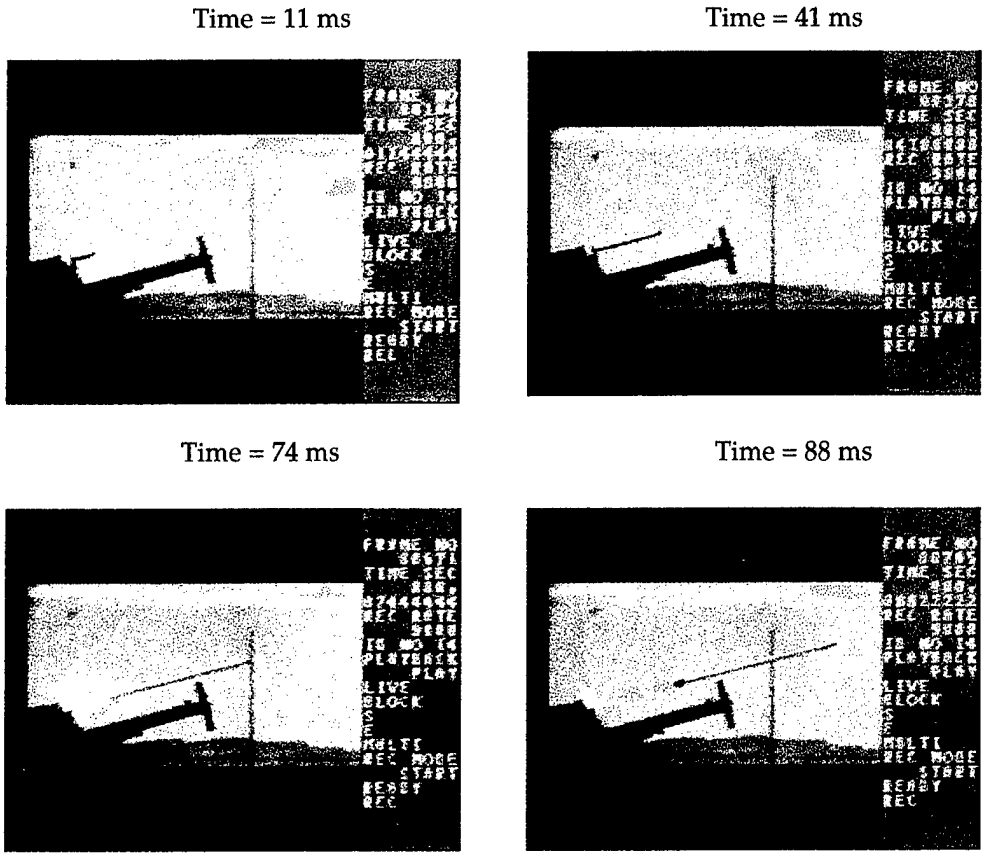

Figure 11. Select Video Images of ARL 1/YPG 15 During Launch.

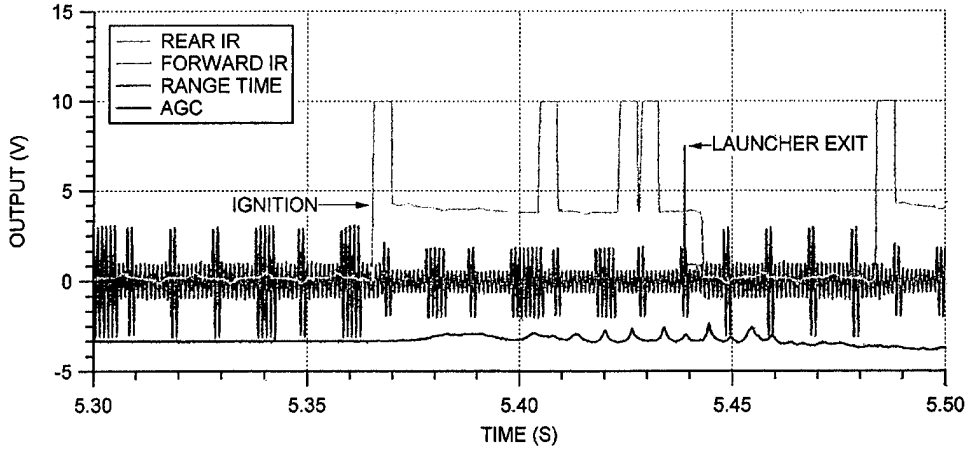

Figure 12. Timing Synchronization Plot.

Table 5. Experimental Measurements

ARL/APL No.	IRIG Time at Ignition (day:hr:min:s)	Time in the Launcher (s)	Launcher Exit Velocity (m/s)	Motor Burn Time (s)	Max Velocity (m/s)	Tiime of Flight (s)	Distance (m)
1	258:16:36:08.3670	0.0735	44.05	1.03	764.10	22.23	6921.7
2	257:17:52:54.0590	0.0729	42.79	1.03	768.54	20.25	6603.7

The data from ARL 1 were superior to those from ARL 2 because a portion of the telemetered data from ARL 2 was missing. Therefore, the data from ARL 1 were fully reduced. With known initial gun conditions (including the gun's location, azimuth, and elevation), the sensor biases and scale factors were applied to the sensor data to convert them into engineering units. Additional spin compensation was performed on the data to correct for biases. Each sensor's data set and reduction process are described in the next section.

6. Relationship Between Earth- and Body-Fixed Coordinate Systems

Since many projectiles rotate while in flight, it is convenient to describe a coordinate system that is fixed to the body. Figure 13 diagrams a body-fixed coordinate system as tied to the IMU. The body-fixed principal axes are described by I, J, and K. P, q, and r are defined as the angular velocities of the j-k axes about the i axis, the k-i axes about the j axis, and the i-j axes about the k axis, respectively. The magnetometer was oriented 18.6 degrees from the -k axis at a radius of 1 inch. The accelerometers were located as close to the roll axis as possible. The rate sensors were located on the -j and k axes. The IMU's location relative to the instrumentation system's exterior was determined by a reference mark 54 degrees from the j axis.

The body-fixed coordinate system, as described before, can be related to an earth-fixed Cartesian coordinate system, such as the east-north-up (ENU) navigation system (see Figure 14). The variables psi (ψ), theta (θ), and phi (ϕ) are used to fully denote the three angular variables required to orient the body's principal axis of rotation and rotation angle within the ENU coordinate system.

Sigma solar (σ_S) and sigma magnetic (σ_M) are defined as the included angles between the body's axis of rotation and the solar and magnetic field vectors whose orientations within the earth-fixed system are known (see Figure 15). The

data reduction techniques to produce the solar and magnetic aspect angles are described in a later section. With knowledge of these measurement angles, Harkins, Davis, and Hepner (2001) have shown that the projectile's pointing vector ($\vec{P}$) can be determined with relative certainty. It is also important to note that the axis of rotation of a spinning projectile is not always collinear with its velocity vector. In this case, an orientation estimate obtained from a time history and from derivatives of location variables does not provide an accurate determination of the pointing vector.

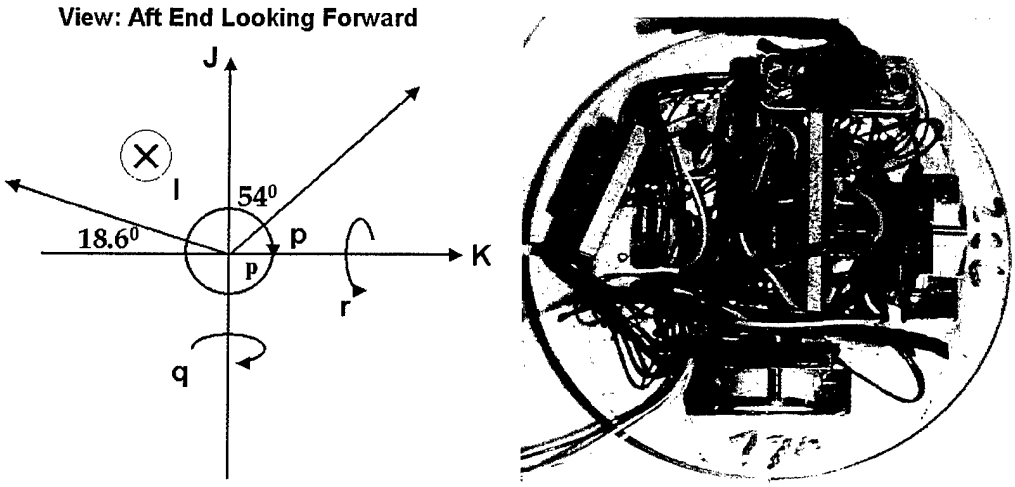

Figure 13. Body-fixed Coordinate System.

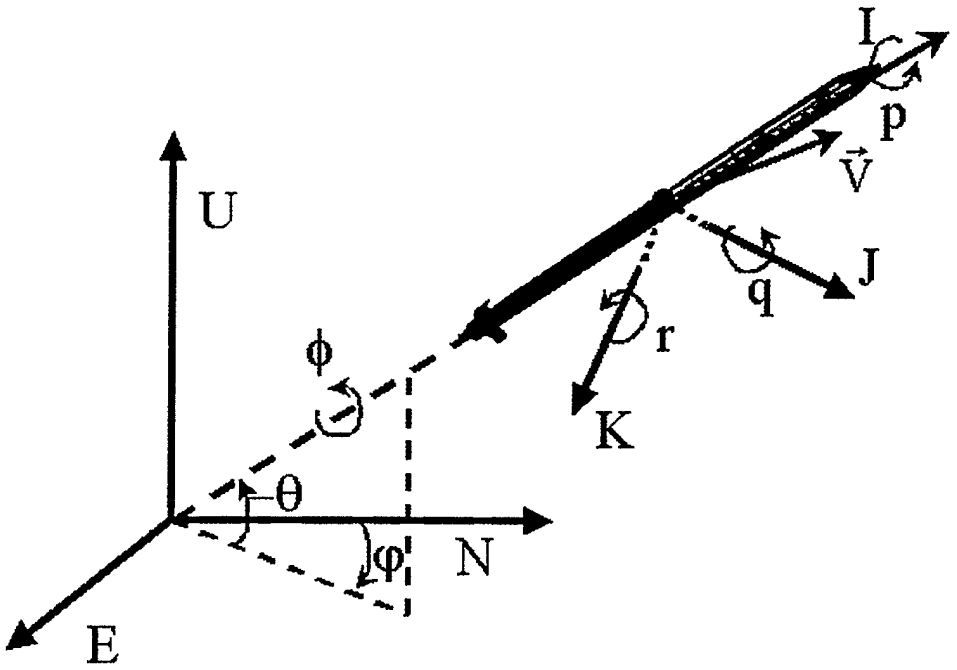

Figure 14. Earth-fixed Coordinate System.

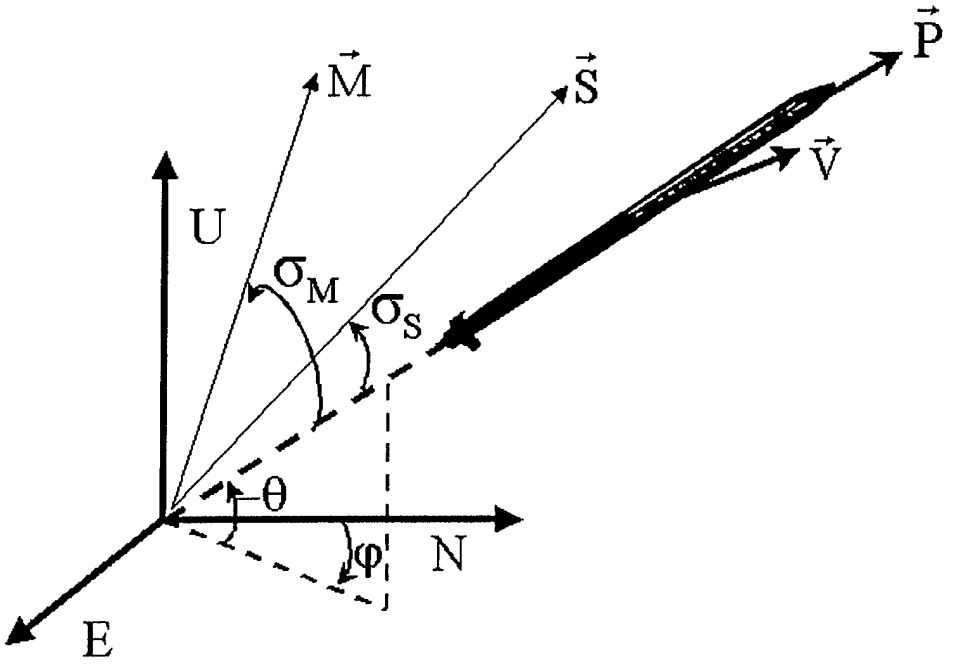

Figure 15. Solar and Magnetic Aspect Angle Descriptions.

7. Flight Demonstration Results

7.1 Accelerometer Data

The sensed accelerations from the axially and radially aligned body-fixed accelerometers on board the rocket can be modeled by Equation 1. Theoretically, the body-fixed accelerometers would be measuring the three components of non-gravitational acceleration (i, j, k) at a point relative to the rocket's c.g. (Δi, Δj, Δk), as seen in Equation 2 (Harkins 1994). For this experiment, the location of the on-board accelerometers was forward of the rocket's c.g. and had some degree of misalignment and misplacement with respect to the principal body axes because of fabrication tolerance limitations and inherent sensor errors.

$$\begin{aligned} \ddot{\vec{H}}_{ia} &= B_a + G_a \ddot{\vec{H}}_i \\ \ddot{\vec{H}}_{ja} &= B_a + G_a \ddot{\vec{H}}_j \\ \ddot{\vec{H}}_{ka} &= B_a + G_a \ddot{\vec{H}}_k \end{aligned} \tag{1}$$

$$\ddot{\bar{H}}_i = \dot{u}_0 - \Delta\ddot{i}_{cg} + q(w_0 - \Delta\dot{k}_{cg}) - r(v_0 - \Delta\dot{j}_{cg}) - g\sin\theta + \Delta i(-q^2 - r^2) + \Delta j(pq - \dot{r}) + \Delta k(pr + \dot{q})$$

$$\ddot{\bar{H}}_j = \dot{v}_0 - \Delta\ddot{j}_{cg} + r(u_0 - \Delta\dot{i}_{cg}) - p(w_0 - \Delta\dot{k}_{cg}) + g\cos\theta\sin\phi + \Delta i(pq + \dot{r}) + \Delta j(-p^2 - r^2) + \Delta k(qr - \dot{p}) \quad (2)$$

$$\ddot{\bar{H}}_k = \dot{w}_0 - \Delta\ddot{k}_{cg} + p(v_0 - \Delta\dot{j}_{cg}) - q(u_0 - \Delta\dot{i}_{cg}) + g\cos\theta\cos\phi + \Delta i(pr - \dot{q}) + \Delta j(qr + \dot{p}) + \Delta k(-p^2 - q^2)$$

in which

$\ddot{\bar{H}}_{i_a}, \ddot{\bar{H}}_{j_a}, \ddot{\bar{H}}_{k_a}$ are the accelerometer's output,

B_a is the accelerometer's zero-g bias offset,

G_a is the accelerometer's gain,

$\ddot{\bar{H}}_i, \ddot{\bar{H}}_j, \ddot{\bar{H}}_k$ are the sensed acceleration components at a point,

p and $\dot{p}$ are the angular velocity and acceleration of the j-k axes about the i axis,

q and $\dot{q}$ are the angular velocity and acceleration of the i-k axes about the j axis,

r and $\dot{r}$ are the angular velocity and acceleration of the i-j axes about the k axis,

v_0, w_0, u_0 and $\dot{v}_0, \dot{w}_0, \dot{u}_0$ are the respective components of translational velocity and acceleration of the pre-launch c.g., and

$\Delta\dot{i}_{cg}, \Delta\dot{j}_{cg}, \Delta\dot{k}_{cg}$ and $\Delta\ddot{i}_{cg}, \Delta\ddot{j}_{cg}, \Delta\ddot{k}_{cg}$ are the velocity and acceleration of the c.g. attributable to a change in location within the projectile as fuel is consumed during rocket thrust.

The raw accelerometer data were converted to engineering units via the scale factor obtained in the laboratory calibration and the zero-g bias measured at the gun site (see Figure 16). The accelerometer biases were verified by the initial conditions while the rocket was in the launcher via the launcher's known quadrant elevation and roll orientation information before launch (see Table 6). The estimated roll rate from the solarsonde reduction was then used to remove the bias attributable to the cross-axis sensitivity of the angular acceleration. This bias is a result of the accelerometer having a slight radial offset from the spin axis and sensing a small percentage of the centrifugal acceleration created during

spin. The ADXL150 "longitudinal" data were clipped when the launch acceleration exceeded approximately 60 g's, so its data for the first second of flight were not valid. A -40-g acceleration load was measured by the launch accelerometer, as seen in Figure 17. It was caused by the detent restraining the rocket's forward motion. Acceleration variation of ±15 g's around nominally measured acceleration can also be seen. The authors are not sure what this represents, but it does not seem to correspond to cross-axis sensitivity to balloting loads or yaw. The accelerometer's performance was severely degraded between 0.5 and 1 second of flight, as seen during an expanded view of the first 1.5 seconds (see Figure 18). The exact cause was not known, but a vibration may have been caused by the rocket motor stuttering because of depleted fuel or by the wrap-around fins that induce a torque opposite the motor nozzle cant. This induced vibration might be occurring at the resonance frequency of the accelerometer, thus causing the poor measurement in this region.

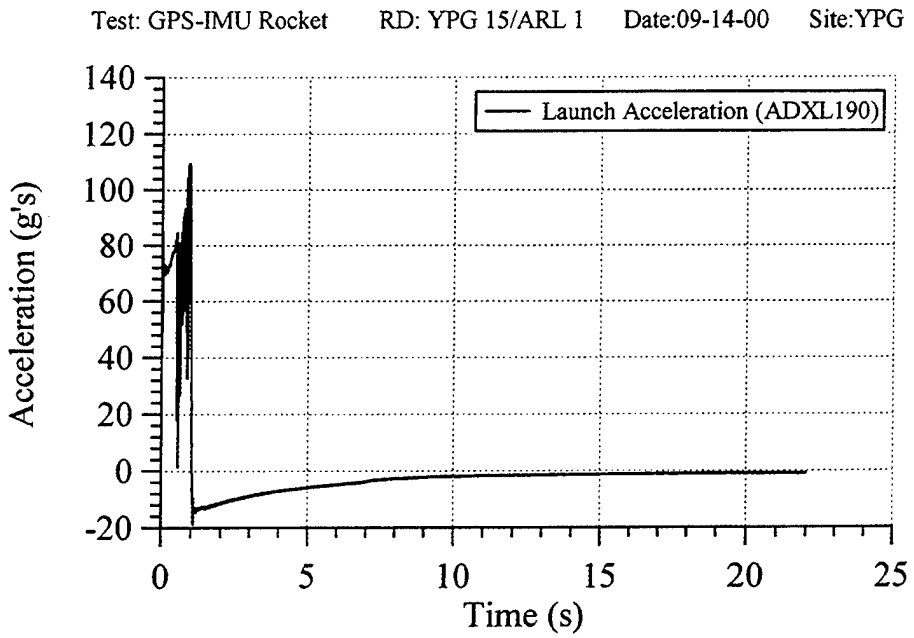

Figure 16. Axial Acceleration.

Table 6. Accelerometer 0-g Bias and Offset Radius Flight Data

Nomenclature (accelerometer)	In Launcher 0g bias (bits)	In Flight Offset Radius (mm)
Launch (ADXL190)	463.15	0.19
Long (ADXL150)	-92.27	0
Horizontal (ADXL250x)	-37.74	0.79
Vertical (ADXL250y)	29.44	-1.48

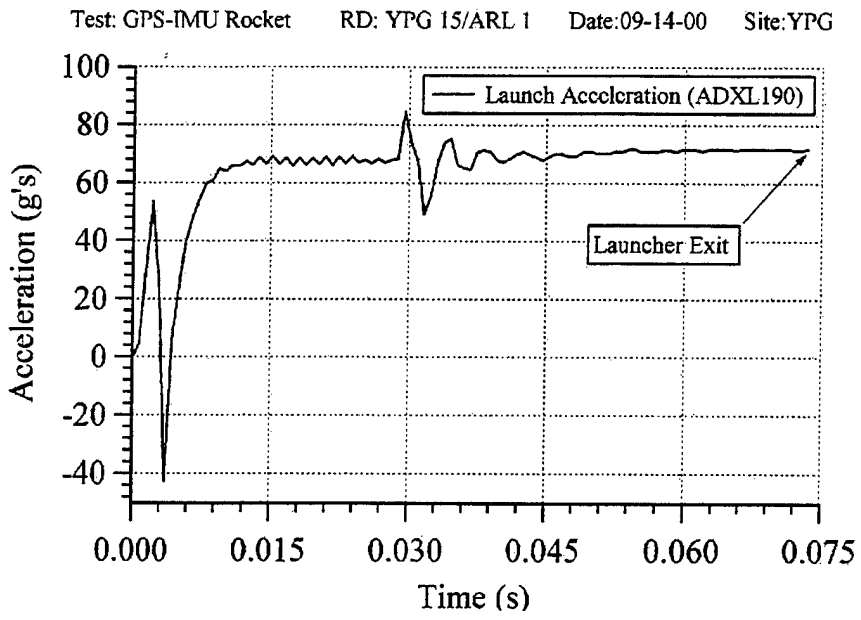

Figure 17. In-Bore Axial Acceleration (0 to 0.0735 s).

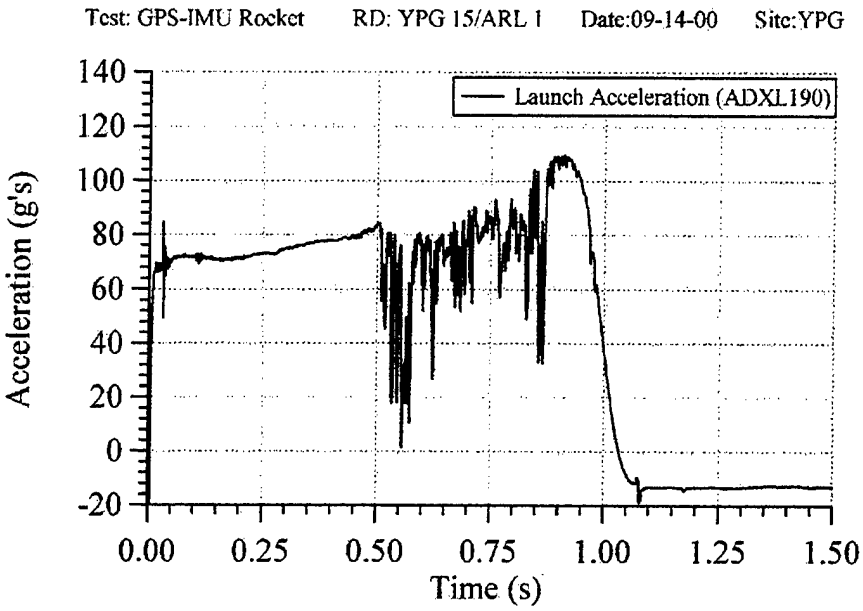

Figure 18. Axial Acceleration (0 to 1.5 s).

The radial "horizontal" and "vertical" accelerometers were also converted to engineering units. Through analysis, it was verified that the accelerometer's radial offsets from the projectiles axis of rotation, as determined in the laboratory, were slightly different from those actually seen in flight. This was probably because of the projectile's geometrical c.g. andthe actual mass center c.g. being slightly different. This would cause the rotational axis of the projectiles to be slightly different in flight. The new radial offsets are shown in Table 6. The radial "horizontal" acceleration and a 1.5-second expanded view are shown in

Figures 19 and 20. High frequency information was present in the radial acceleration from 0.5 to 1 second as well. From 1 to 4 seconds, the radial acceleration data shows a damped oscillating output of 5 g's peak amplitude with a frequency near 20 Hz. The accelerometers are reacting to the projectile's q and r body rates while being modulated by a combination of the spin rate p plus this yawing frequency. This interpretation is validated by the magnetometer and angular rate sensor measurements discussed later in this section.

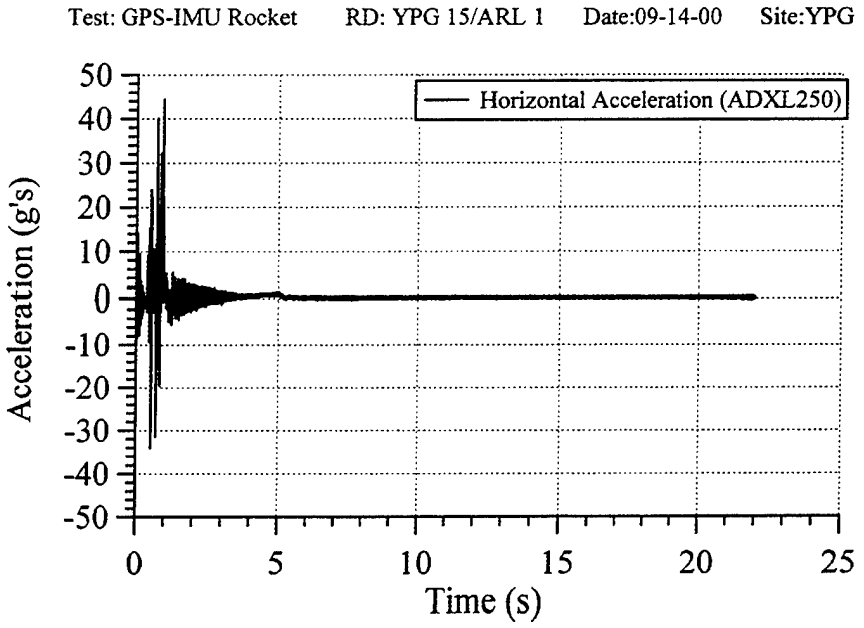

Figure 19. Radial Acceleration.

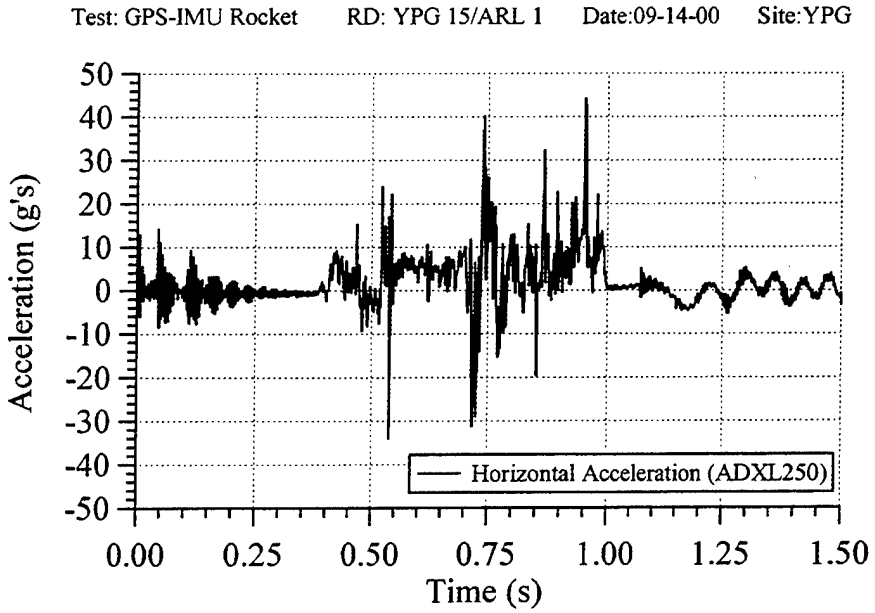

Figure 20. Radial Acceleration (0 to 1.5 s).

7.2 GPS Data

The GPS data were reduced by APL. The GPS processing techniques are more fully described in a separate report by Asher et al. (2000). In summary, a preliminary non-coherent differential GPS solution was constructed with the extracted L1 carrier frequency coarse/acquisition (L1 C/A) code experimental data. The data were sampled at 40 Hz and were then processed via a Kalman filter smoother to produce an initial trajectory. The last smoothing step was non-causal, meaning that the estimates of position, velocity, and acceleration are optimized to fit all the data (past, present, and future) so that the position, velocity, and acceleration estimates can and will actually anticipate data (e.g., the GPS velocity may be nonzero; yet the rocket was at rest). It was estimated that the initial trajectory position data had a 2-m 1-σ accuracy. The data were reduced in ENU and earth-centered earth-fixed coordinates. Figures 21 and 22 show the position and velocity in ENU coordinates. The ENU position started from the rocket's initial location at YPG (3993.23 m north, 645.377 m east, -50.21 m up) relative to an origin that was located at the phase center of the reference antenna.

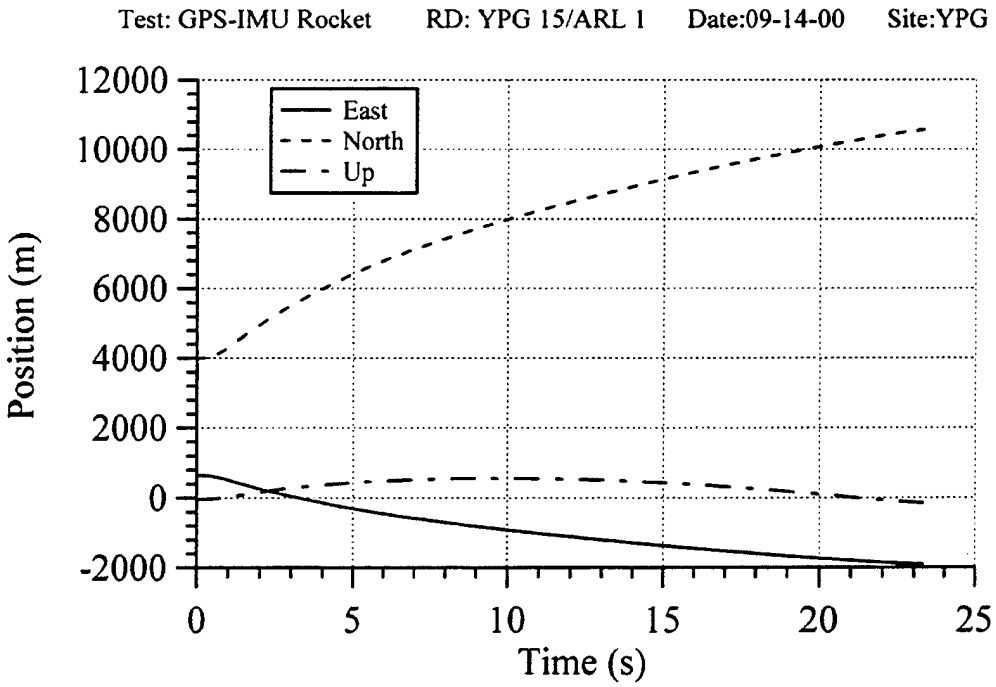

Figure 21. GPS Position Components.

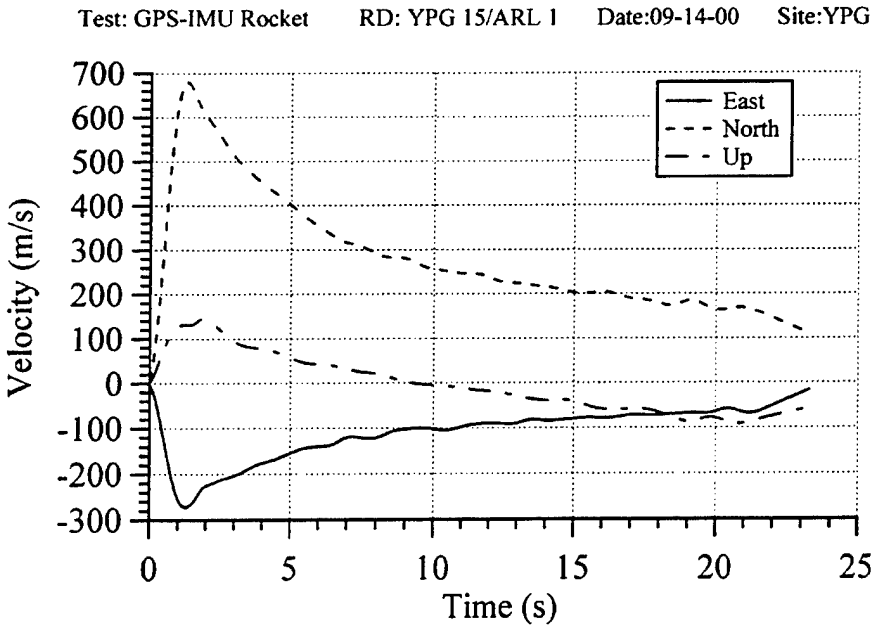

Figure 22. GPS Velocity Components.

7.3 Accelerometer and GPS Comparisons to Radar Data

Since an accelerometer in free fall cannot sense gravity, a gravity term equal to $g(\sin \theta)$ was added to the accelerometer's measurement before it was integrated. Theta is derived from the radar data but could also be determined by the magnetometer and solarsonde measurements. The integrated axially aligned ADXL190 accelerometer data, along with the GPS velocity data, were then compared to the radar (see Figure 23). The Hawk radar data and Weibel radar data were nearly identical, so only the Weibel was used as the truth measurement for comparisons. The accelerometer data from the first 0.0735 second were integrated to obtain an estimated launcher exit velocity of 47 m/s (see Figure 24). The accelerometer-derived velocity differed by 3 m/s from the launcher exit velocity, as measured by the radar.

The accelerometer-derived velocity differed by as much as 28 m/s from the radar-derived velocity during the 1-second boost phase (see Figure 25). This difference was a direct result of the corrupted data causing vibration-induced error, which occurred between 0.5 and 1 second. Once the accelerometer's integrated velocity was reinitialized at the 1-second mark, it differed by about 5 m/s throughout most of the flight until the last 7 seconds when it differed by as much as 17 m/s (see Figure 26). The GPS data differed from the radar data by as much as 20 m/s. This difference was mainly at the rocket's acceleration transition from thrust to drag. After discussion with APL, it was determined that this was a direct result of the way the GPS data were processed. The Kalman smoother acted like a filter, and the sharp velocity slope change at rocket burnout was rounded.

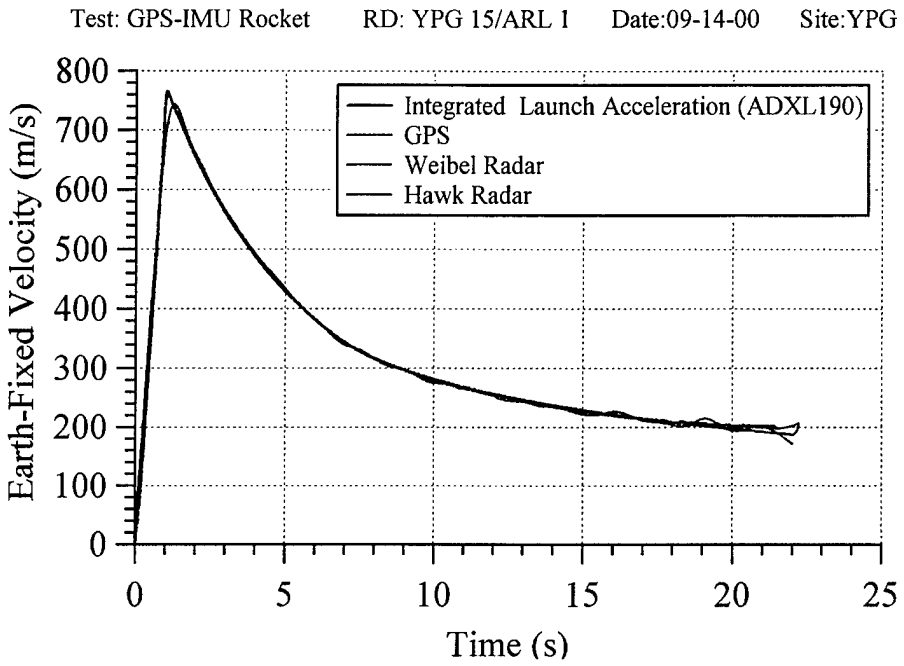

Figure 23. Velocity Comparison.

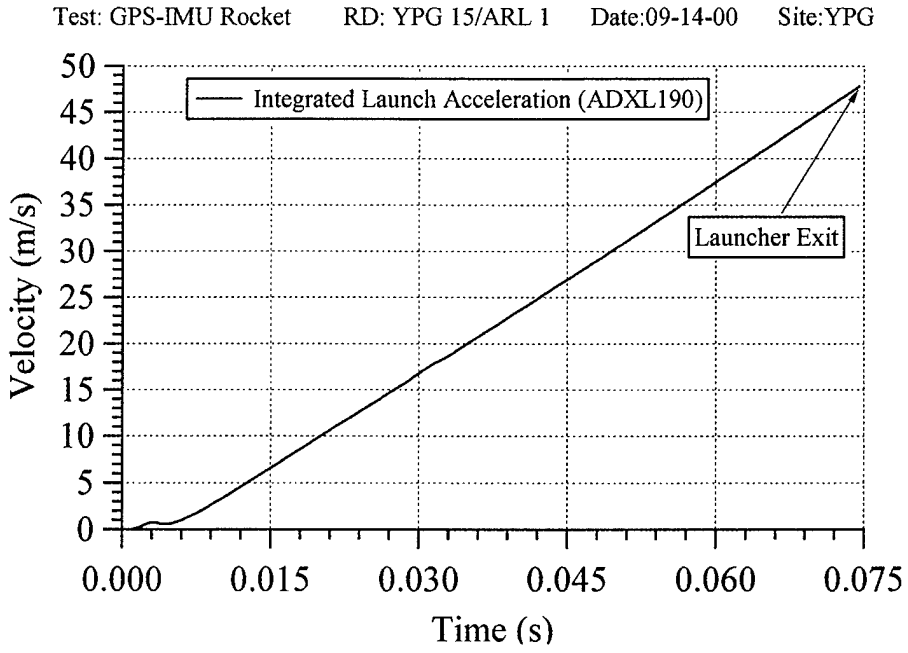

Figure 24. Velocity (0 to 0.0735 s).

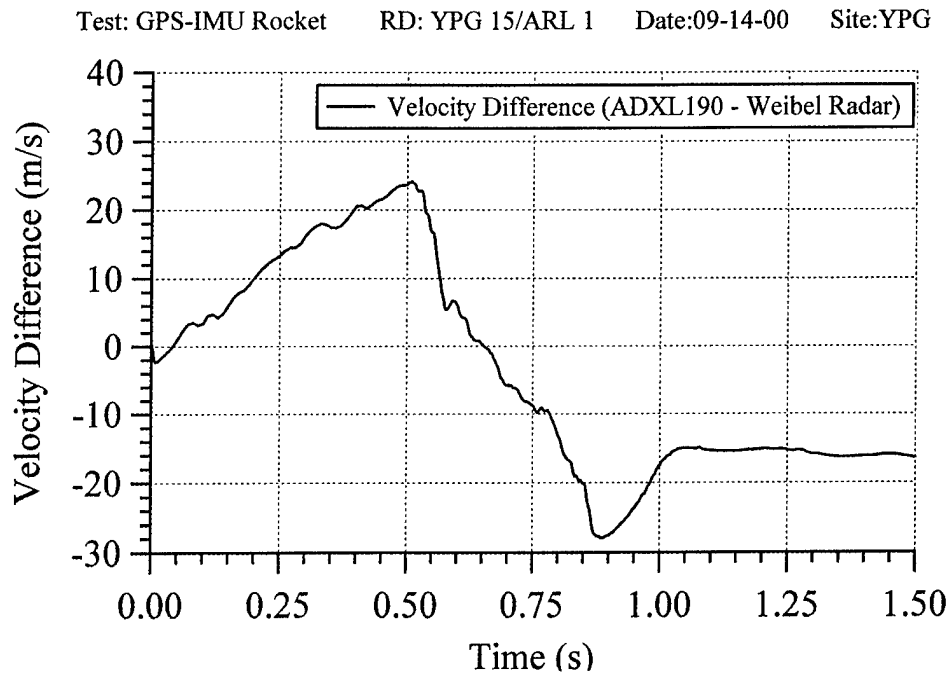

Figure 25. Velocity Difference (0 to 1.5 s).

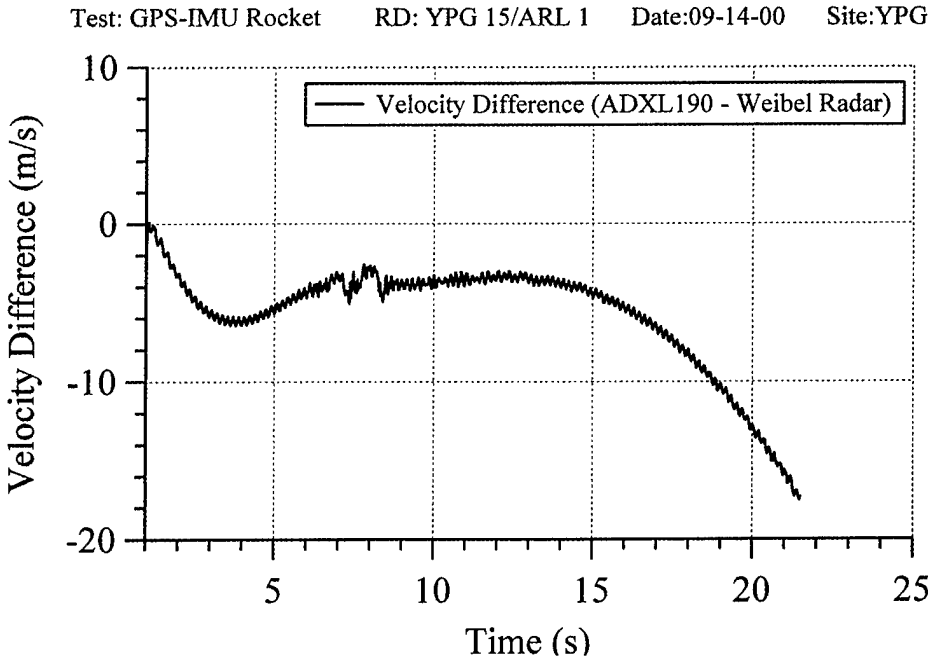

Figure 26. Velocity Difference (2 to 20 s).

Next, the axially aligned accelerometer data were integrated twice to obtain the distance traveled along the flight path. The flight path distance from all the data sources is shown in Figure 27. The Weibel radar position data and GPS position

data agreed to within 10 m throughout the entire flight. However, there was a 115-m distance difference by flight's end between the doubly integrated accelerometer data and the Weibel radar position data (see Figure 28).

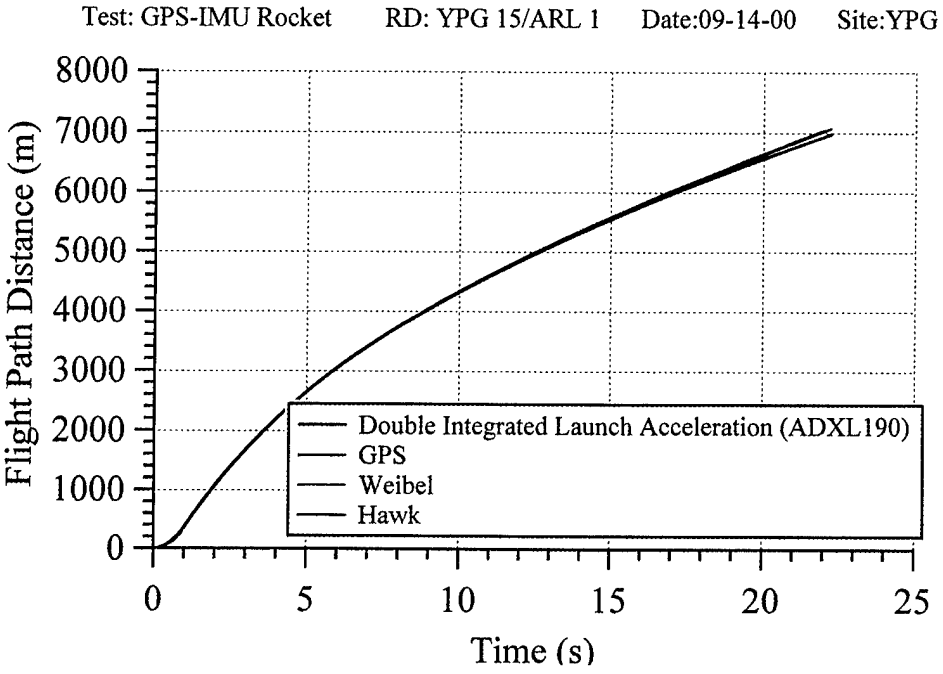

Figure 27. Flight Path Distance Comparison.

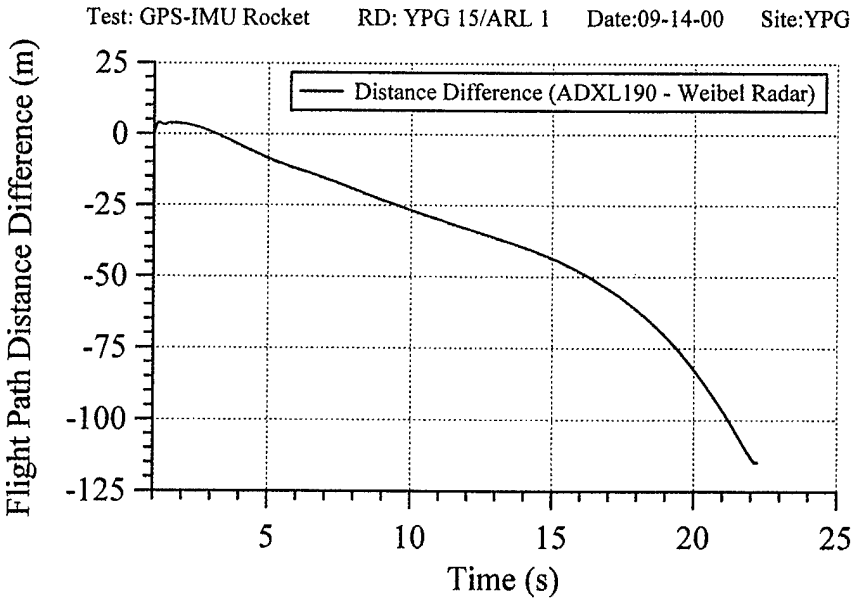

Figure 28. Flight Path Distance Difference.

7.4 Magnetometer Data

The magnetometer's output while on board a rotating freely flying body can be expressed in a conveniently defined coordinate system by Equation 3:

$$O_M = (G_M)|M|[\cos(\lambda_M)\cos(\sigma_M) + \sin(\lambda_M)\sin(\sigma_M)\sin(\phi_M)] + B_M \quad (3)$$

in which

O_M = magnetometer output,

G_M = the magnetometer's gain,

$|M|$ = the ambient magnetic field strength,

λ_M = the angle between the magnetometer's sense axis and the spin axis,

ϕ_M = the roll orientation of the projectile, and

B_M = the no-field bias offset.

The axially and radially oriented magnetometer raw data from ARL 1 are plotted in Figures 29 and 30. The axially oriented magnetometer data, after having their bias offset and scale factor applied, should have been a direct measure of the angle to the magnetic field. Unfortunately, the magnetometer data were attenuated, and a large cross-axis sensitivity was evident in the data. It was determined that this was attributable to the intrinsic nature of the permalloy thin film sensing material used in the magnetometer device. The device has indigenous "on-chip" magnetically coupled straps (set/reset and offset) to ensure repeatability of the bias offset, scale factor, and alignment. Unfortunately, the set/reset and offset straps were not used in this experiment. For comparison, the axially and radially oriented magnetometer raw data from ARL 2 are plotted in Figures 31 and 32. This magnetometer worked as intended.

The radially oriented magnetometer from ARL 1 was not affected as much as the axial magnetometer but still had problems associated with its scale factor and bias changing since the laboratory calibration. The radially oriented flight data could still be processed to determine the amplitude and frequency of the magnetometer data. The resulting frequency measurement represents $\dot{\phi}_M$, that is, the roll rate with respect to the earth's magnetic field. This is related to the actual roll rate by the following equation:

$$\dot{\phi}_M = p + r\tan(90 - \sigma_M) \quad (4)$$

$\dot{\phi}_M$ is exactly equal to p when there is no yawing motion or when the projectile's instantaneous σ_M angle is 90 degrees. For ARL 2, the axially oriented magnetometer data were properly scaled and the bias shifted, based on initial launch conditions to directly obtain σ_M. For ARL 1, the amplitude envelope of the

radially oriented magnetometer data was used to obtain σ_M. Unfortunately, the geometry of the experiment made the radially oriented magnetometer very insensitive to aspect angle change, and the first 7 seconds were not considered reliable. Since the scale factor and bias from ARL 1 were different from those obtained in the laboratory, they were adjusted until the σ_M overlaid that of ARL 2. The processed estimated roll rate and magnetic aspect angle from both ARL 1 and 2 are plotted in Figures 33 and 34.

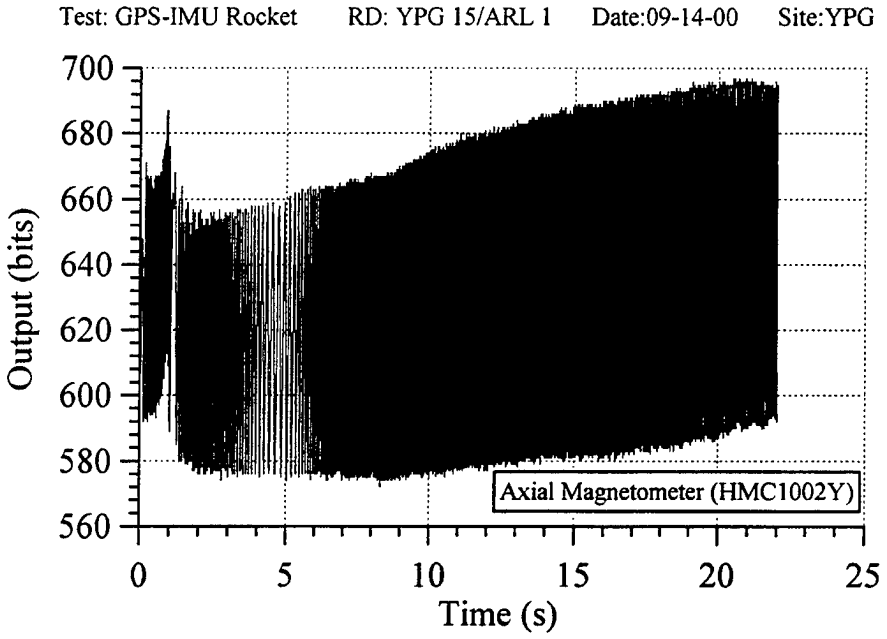

Figure 29. Axially Oriented Magnetometer Data for ARL 1.

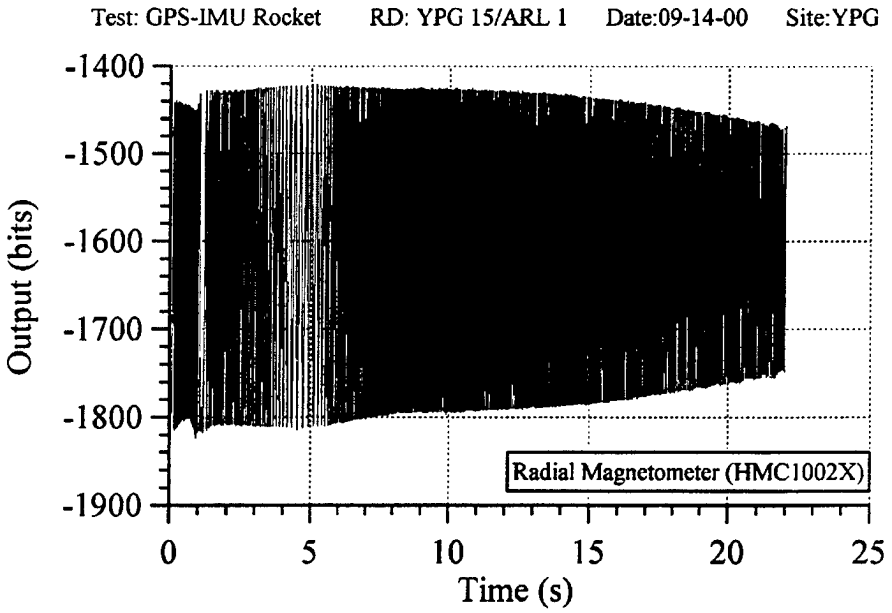

Figure 30. Radially Oriented Magnetometer Data for ARL 1.

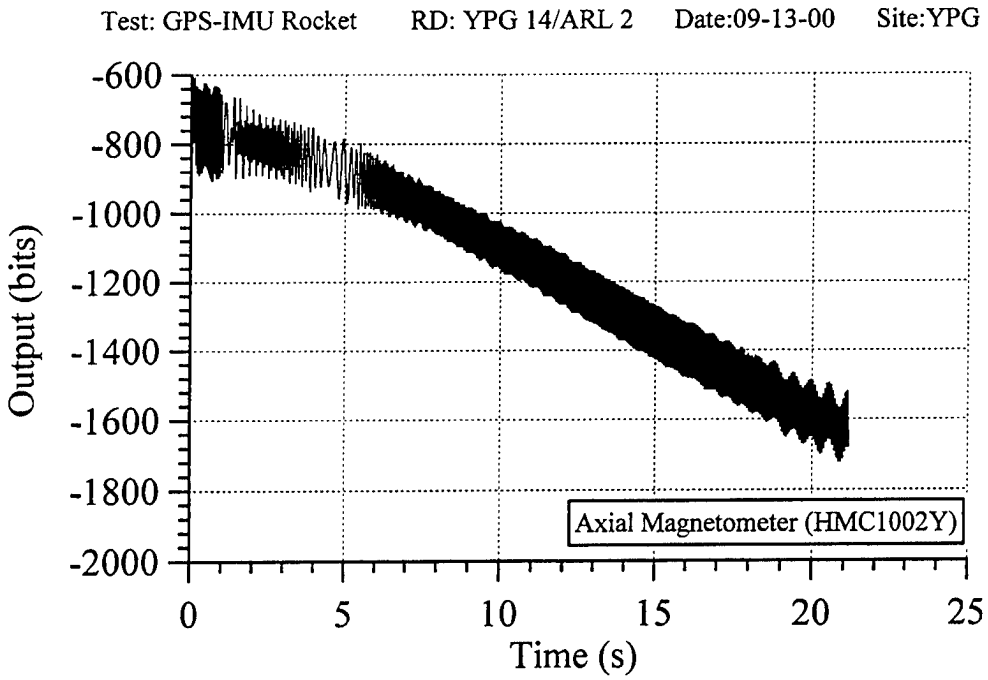

Figure 31. Axially Oriented Magnetometer Data for ARL 2.

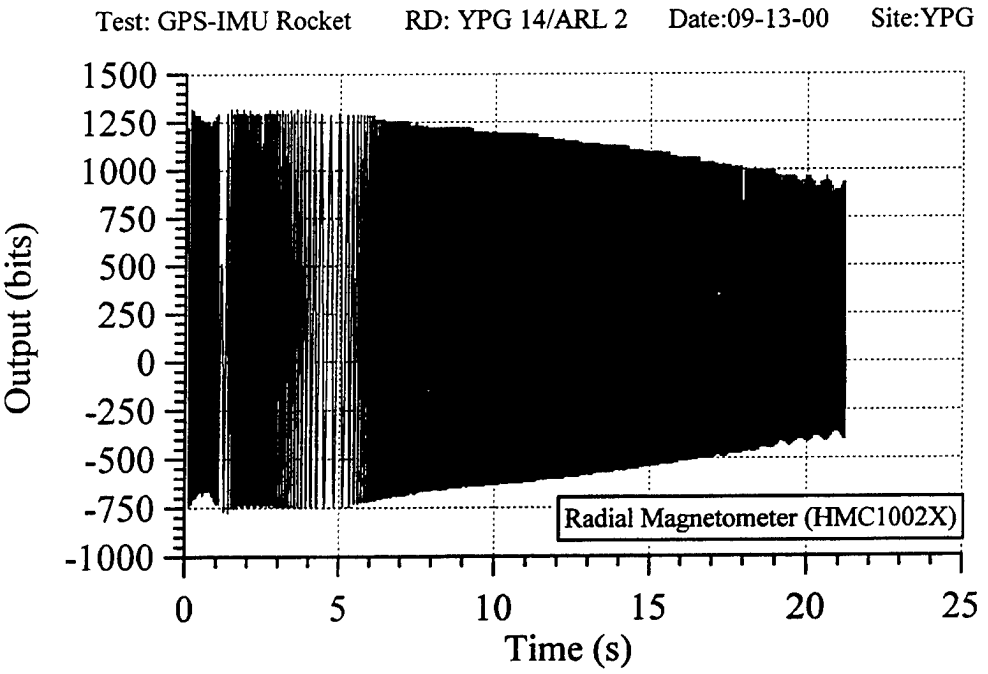

Figure 32. Radially Oriented Magnetometer Data for ARL 2.

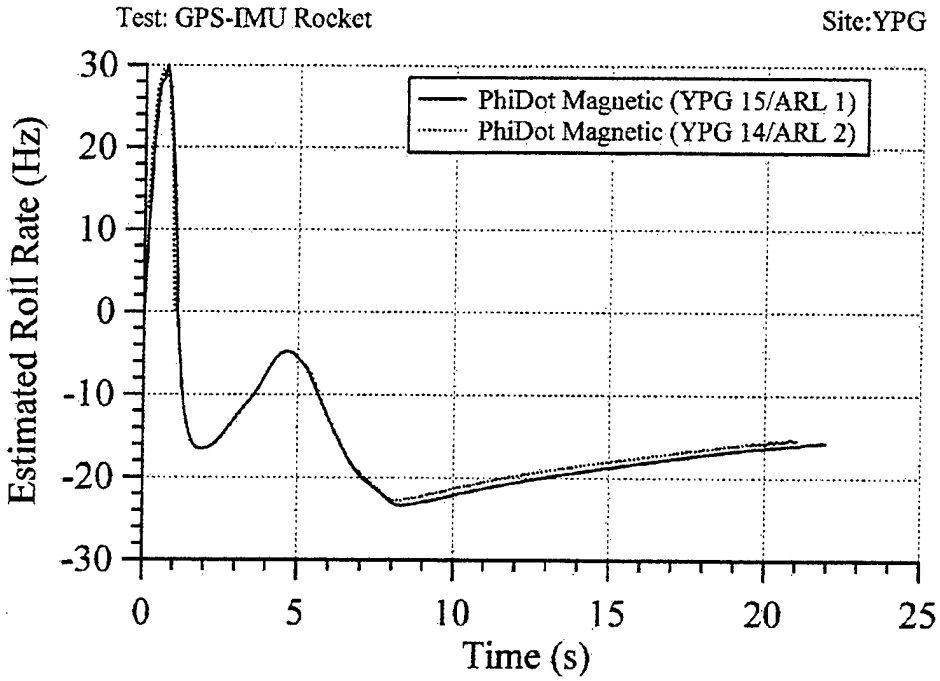

Figure 33. Estimated Roll Rate Via Magnetometer Data.

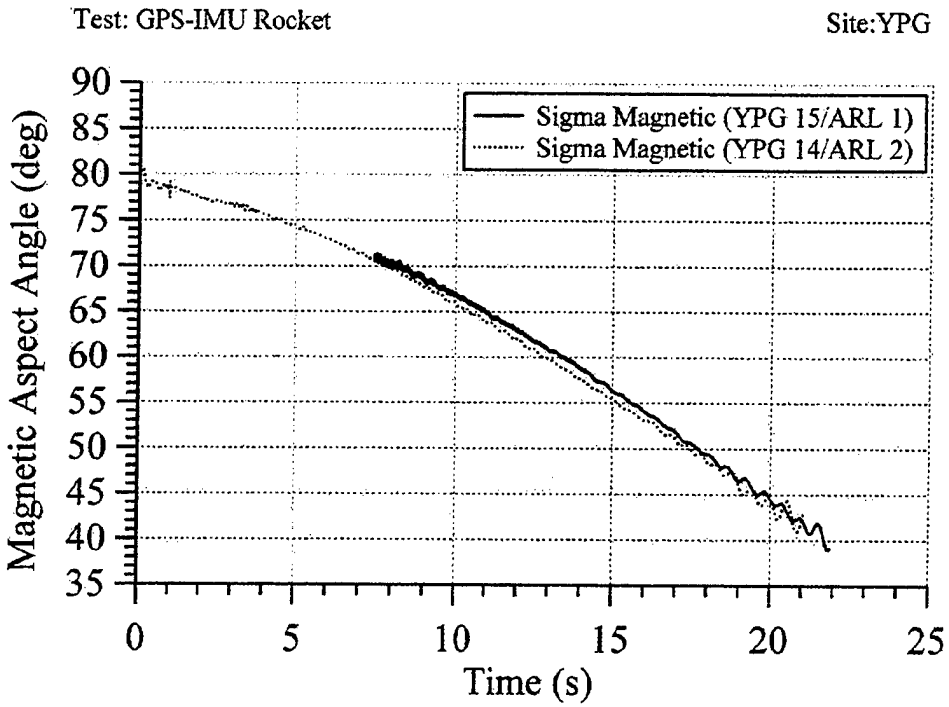

Figure 34. Magnetic Aspect Angle.

7.5 Rate Sensor Data

The angular rate sensors used were of a magneto-hydro-dynamic (MHD) type. When these sensors were fixed to a maneuvering rocket, the angular rotation of the sensor's magnetic case results in relative velocity to an annulus of conductive fluid. Motion in the field produces voltage across the conductor proportional to the relative velocity, according to Faraday's Law. Therefore, a relative motion of the fluid with respect to the rocket causes a proportional output. Conversely, if there is no relative motion, there is no output.

The pitch and yaw rate MHD sensors experienced small bias shifts before launch. The pitch and yaw rate data were corrected for bias offsets of -8.23 deg/s and -16.45 deg/s, respectively, as seen in the flight data before launch. These biases were most likely associated with the electronic conditioning of the output signal or a telemetry problem and were not an artifact of the sensor. The angular rate data after bias correction are shown in Figures 35 and 36. The output from the yaw rate sensor is different than that of the pitch rate sensor. The polarity of the output between the two sensors is opposite. There seems to be a bias error that tracks with the roll rate in both sensors but it is much more noticeable in the yaw rate sensor.

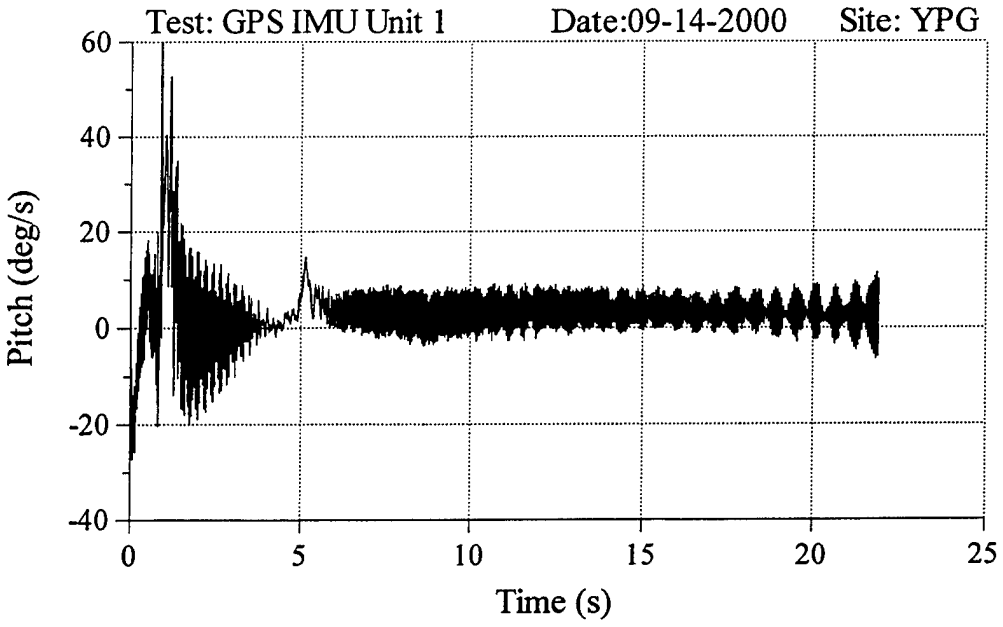

Figure 35. Pitch Angular Rate.

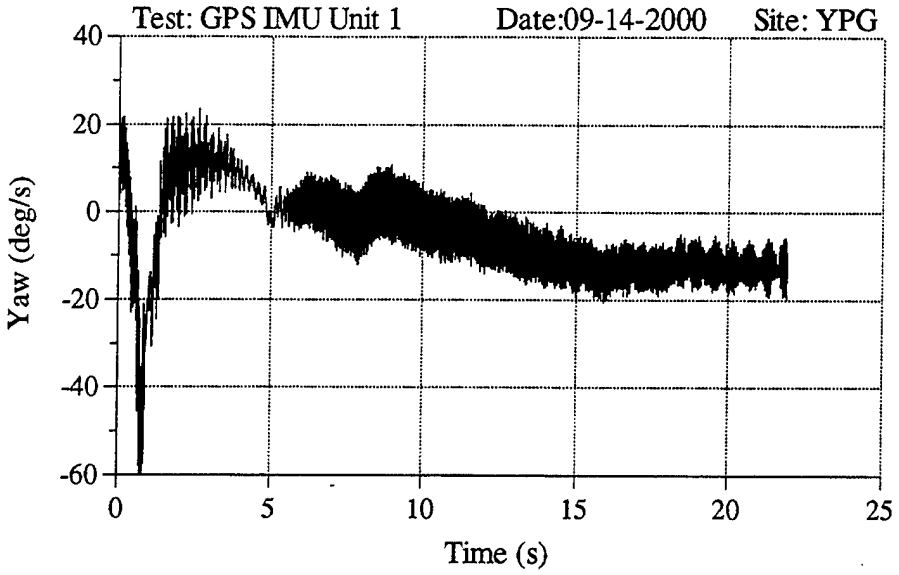

Figure 36. Yaw Angular Rate.

The angular rate sensors were able to provide the angular rates of the rocket for the launch portion of the experiment. Figure 37 depicts a representative history of the angular pitch rate before, during, and after launcher exit. As mentioned earlier, time zero is with respect to rocket ignition at t = 0.0 s. Notice that the peak angular rate measured immediately after rocket ignition was -17 deg/s. This was most likely caused by the release from its detent. The angular rate at launcher exit was -8 deg/s.

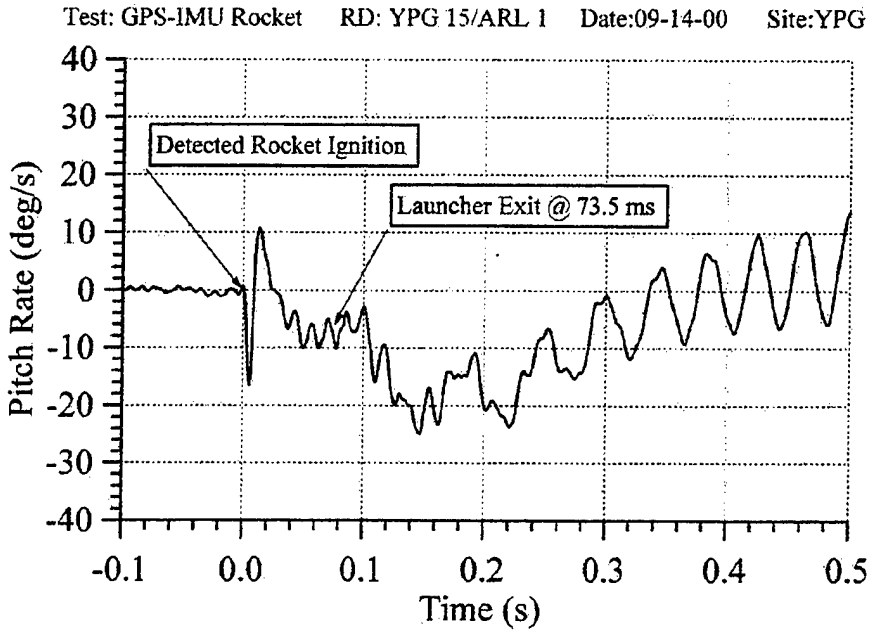

Figure 37. Pitch Rate (0 to 0.5 s).

7.6 Rate Sensor and Magnetometer Comparisons to Solarsonde Data

The SLIT sensors were included in the flight demonstration as an independent measure of the rocket's angular data as well as to provide a truth measurement for the rate sensor and magnetometer data. The solar sensors provided positive and negative pulse train data from four optical sensors, which are related to the projectile's roll and yaw histories along the entire trajectory with respect to the sun. These processed data produce solar roll rate ($\dot{\phi}_S$) and the solar aspect angle (σ_S) data with accuracies of 0.05 Hz and 0.10°, respectively. The σ_S is similar to the aforementioned magnetic heading angle described in Section 7.4 but is measured with respect to the sun and is used as the truth measurement for this experiment. For this experiment, four optical sensors were required to satisfy basic sampling theory. The $\dot{\phi}_M$ was compared to the $\dot{\phi}_S$ in Figure 38. The average difference was approximately 0.1 Hz, suggesting that the magnetometer approach for roll rate estimation is a good technique and can be relied upon as a replacement for solarsonde when the sun is not available. Comparisons of the magnetic and solar aspect angles to their respective field were made in Figure 39. The amplitude of the large angular deviation that was observed in the solarsonde σ_S data at 1 second was not considered to be real. This is because the solarsonde processing requires a sufficient sampling rate. Since the roll rate was nearly zero at that instant, the criterion for valid data was briefly violated. This is consistent with the other data sources since the magnetometer and radial accelerometer did not indicate a large angular deviation at 1 second. The peak-to-peak motion about the centerline of both sigma data sets was consistent.

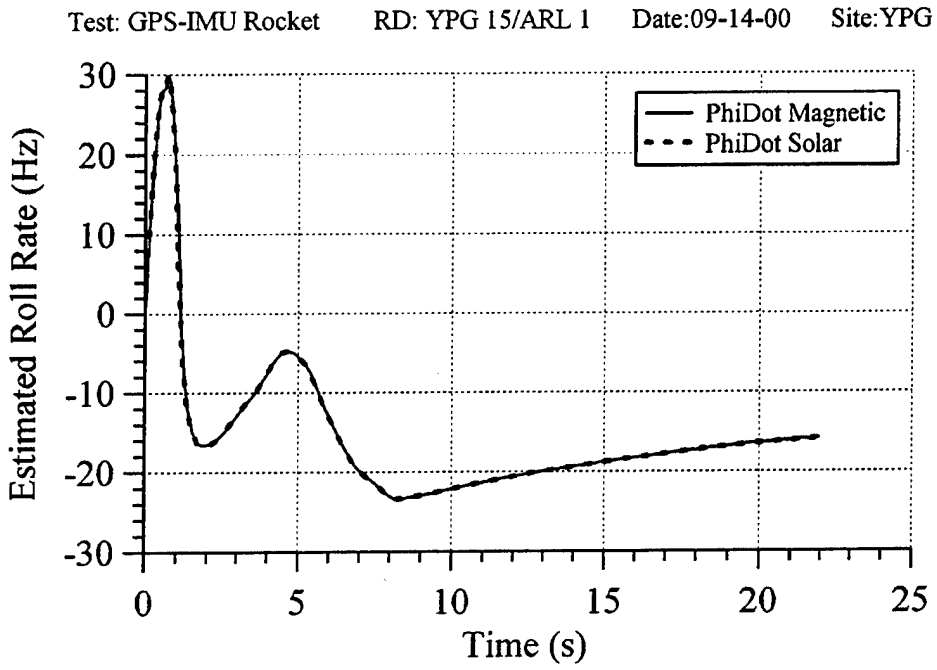

Figure 38. Roll Rate Comparison.

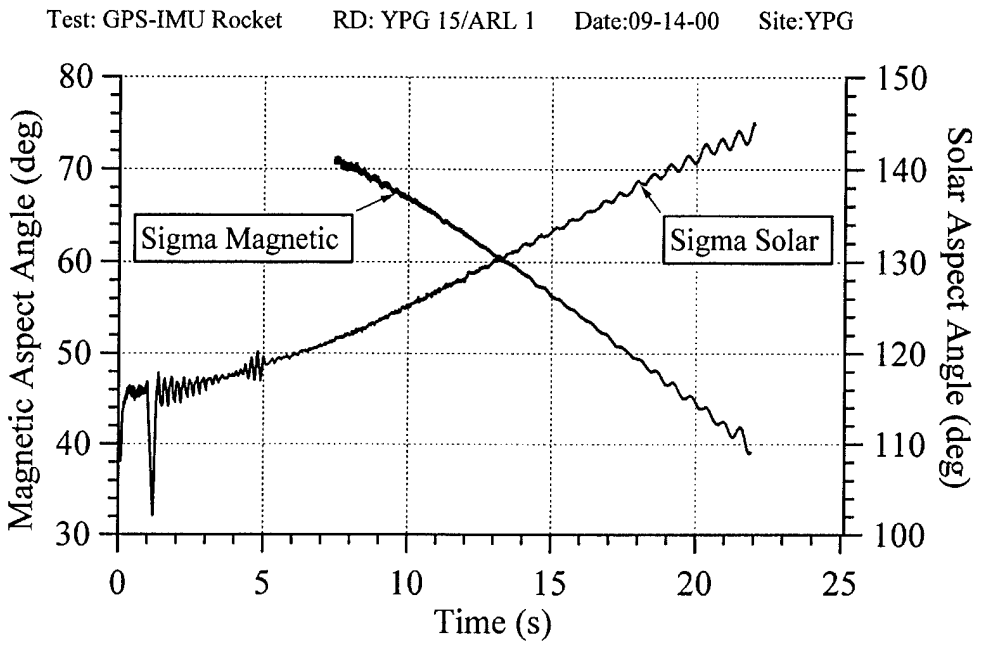

Figure 39. Aspect Angle Comparison.

Quantitatively, the output from the MHD-type angular rate sensors was compromised at times because of problems that were encountered during the experiment and because the sensor was ill suited to make accurate measurements on this particular rocket platform because it was improperly selected by the authors. Qualitatively, useful information was contained in the data. The character of the data agrees with expectations for angular motions in free flight. For instance, during the terminal portion of the flight when the rocket was in a limit cycle, the pitch and yaw rate sensors produced amplitude-modulated output, as displayed in Figure 40. Looking at the angular rate motion in Figure 40, we see that the angular motion of the rocket was about 5.5 deg/s from 20 to 21 seconds. This rate is close to a rate of 5 deg/s, as derived from the solar aspect angle data over the same time period. At a flight time of 2 seconds, the pitch and yaw rate measurements are 17 deg/s and 12.5 deg/s, respectively. This corresponds to the derivative of the solar aspect angle data of roughly 12 deg/s over the same time period, which suggests reasonable agreement. This angular rate history is very close to what was anticipated during 6-degree-of-freedom trajectory simulations. No comparison to trajectory simulation is presented here, but simulations made for similar flight bodies compared well to actual rate sensor data.

Next, a comparison of the frequency content was made between the post-processed MHD and SLIT sensor measurements. Figures 41 and 42 show good agreement between the average MHD pitch and yaw rate sensor frequency to the solar roll rate frequency from 5 seconds through impact. When angular motion was present, especially at the end of the rocket's flight when it was in a limit

cycle, the rate sensor frequency should have approximated the roll rate with an oscillation superimposed on it that was a function of the angular rate and its direction. As the motion of the rocket became more excited, the frequency as measured by the rate sensor had even higher oscillation content. This oscillation is a direct measure of the angular rate frequency.

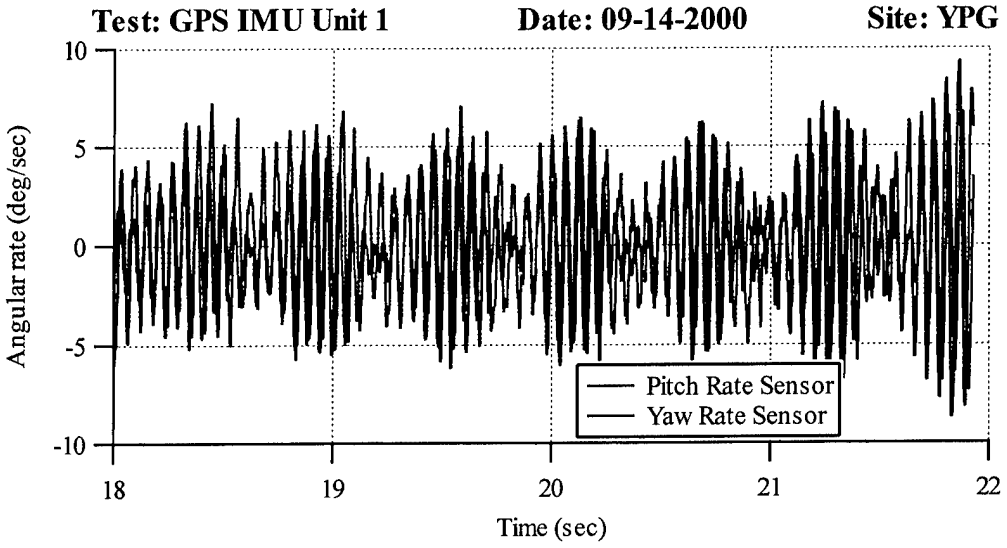

Figure 40. Angular Rate (18 to 22 s).

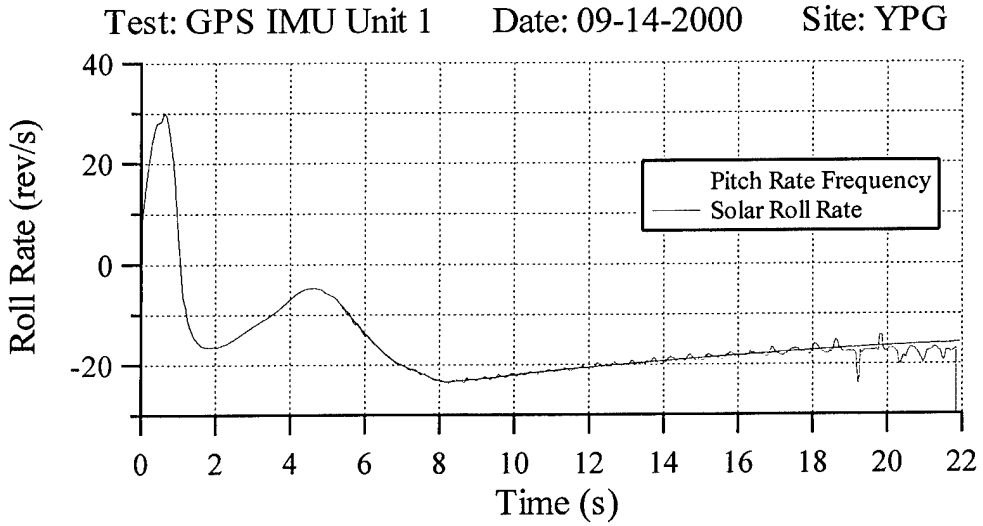

Figure 41. Pitch Rate Frequency Compared to Solar Roll Rate.

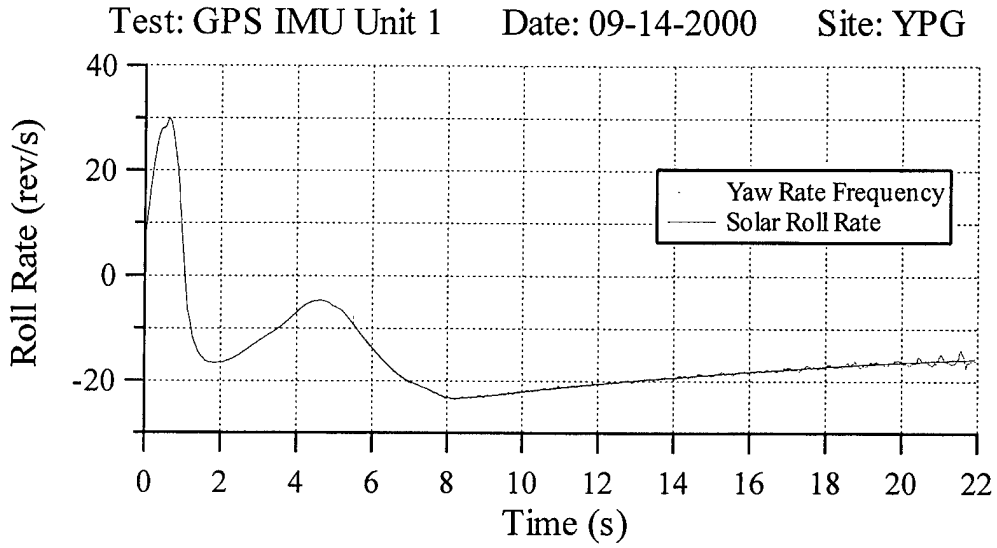

Figure 42. Yaw Rate Frequency Compared to Solar Roll Rate.

8. Aerodynamic Coefficient Analysis

The techniques and equations used by Arrow Tech Associates (Arrow Tech) to derive a projectile's aerodynamic coefficients from its down-range velocity and angular motion history were first documented by Whyte, Houghton, and Hathaway (1973). Arrow Tech worked with ARL to turn this technique into the PC Yawsonde program (1993). It uses the projectile's velocity, position, and antenna angular orientation data from the radar along with the solarsonde angular motion data as input into the program. Brown, Brandon, Harkins, and Hathaway (1997) used this technique to estimate the drag and moment coefficients of a 2.75-inch rocket.

As part of this demonstration, Arrow Tech was contracted by ARL to determine how well the aerodynamic coefficients of the instrumented 2.75-inch rockets could be estimated with the GPS and IMU data. The new approach, called telemetry, radar, yawsonde data, and analysis system (TRYDAS), as reported by Hathaway et al. (2000), incorporates the additional data from the GPS and on-board inertial sensors. ARL supplied Arrow Tech with the following data necessary to do the analyses: projectile physical properties, experimental setup information, meteorological data, radar velocity, radar position, sensor output versus time, GPS velocity, and GPS position. It is important that a common time reference of all data sources be obtained. In addition, a complete estimated aerodynamic coefficient file was constructed with Arrow Tech's PRODAS 2000 computer software code (see Appendix C). The coefficient table provided an initial guess and alleviated the analytical complexities of modeling coefficients as

Mach number. An estimated rocket thrust table was also supplied. The complete set of data requirements for the aerodynamic reduction process is included in Appendix D.

To verify the PRODAS model, a trajectory match to the ARL 1 flight data was attempted. In order to exactly match the position and velocity data, the thrust table values were multiplied by a form factor of 0.9, the drag coefficient values were multiplied by a form factor of 1.1, and an initial pitch "tip-off" rate of -0.17 rad/s was required. In all, the PRODAS model provided a good start for Arrow Tech to proceed.

9. Conclusions

ARL and APL have learned many lessons from these experiments. For instance, the accuracy of the inertial sensor and GPS flight data, as compared to radar and solarsonde truth data, was investigated and reported. Also, errors and complexities associated with sensor location and alignment within the flight vehicles, calibration, and time synchronization between the various measurement sources were measured and are now better understood. IMU and GPS data, combined with the solarsonde and radar data obtained from this instrumented rocket demonstration, were the first such data set available to determine aerodynamic force and moment coefficients by the TRYDAS technique. Arrow Tech has been working with the flight data set and will be reporting about the accuracy of using these additional data sources as input to obtain aerodynamics, as compared to the PC yawsonde technique that uses just radar and solarsonde data.

Although HSTSS did not continue to fund the GPS translator evaluations, APL is planning to further analyze the data from this experiment, and it is trying to incorporate the GPS translator into other imminent flight demonstrations. Additional flight demonstrations with rockets and other types of munitions instrumented with inertial sensors are also under way at ARL. The IMU designs have been improved to include both MEMS accelerometers and MEMS rate sensors. The signal conditioning and signal post processing of the magnetometer measurements have been modified. Instead of amplitude-calibrated magnetometer data, a patent pending method called MAGSONDE, as reported by Hepner and Harkins (2001), can sometimes provide an accurate measurement of the angular orientation of a spinning body with respect to the earth's magnetic field from unique processing of the phase information from a radially oriented and a tilted pair of magnetometers.

The success of using low-cost COTS IMUs and GPS translators in projectiles for reconstructing trajectories implies that these low-cost IMUs could be combined

with GPS to provide tactical guidance via tightly coupled or deeply integrated INS/GPS solutions. Draper Laboratory, under a Navy contract, is set to demonstrate such a low cost guidance electronics unit concept, using a similar set of IMU devices combined with a GPS receiver for extended range guided munitions. Several other Army and Navy programs are looking into the use of MEMS inertial sensors for tactical guidance.

INTENTIONALLY LEFT BLANK

References

Arrow Tech Associates, "PC-Yawsonde Technical User's Manual," South Burlington, VT, 1993.

Arrow Tech Associates, "PRODAS 2000 Technical User's Manual," version 2.2.16. South Burlington, VT, 1999.

Asher, M., L. Linstrom, M. Boehme, G. Moore, D. Duven, E. Olsen, W. D'Amico, R. Denissen, and W. Devereaux, "Post-flight Trajectory Reconstruction of a 70-mm Rocket Using a Miniaturized GPS Translator," 2000 GPS Users' Conference, JSDE Session, Oxnard CA, October 2000.

Burke, L., E. Bukowski, C. Newnham, N. Scholey, W. Hoge, and Z. Ye, "HSTSS Battery Development for Missile and Ballistic Telemetry Applications," U.S. Army Research Laboratory, Aberdeen Proving Ground, MD, ARL-MR-477, May 2000.

Brown, T.G., F. Brandon, T. Harkins, and W. Hathaway, "Drag and Moment Coefficients Measured During Flight Testing of a 2.75-inch Rocket," AIAA 97-0634, 35th Aerospace Sciences Meeting & Exhibit, Reno, Nevada, January 1997.

Brown, T.G., and B.S. Davis, "Commercial Technology Insertion Program: Military Ground and Flight Experimentation with MEMS Sensors at the U.S. Army Research Laboratory," U.S. Army Research Laboratory, Aberdeen Proving Ground, MD, ARL-TR-2073, December 1999.

Condon, J.A., "A Mechanical Design for an Inertial Measurement Unit (IMU) for 2.75-inch Rockets and Missiles," U.S. Army Research Laboratory, Aberdeen Proving Ground, MD, ARL-MR-456, July 1999.

Davis, B.S., T.G. Brown, C. Myers, and M.S.L. Hollis, "Ground and Flight Testing of Microelectromechanical Systems (MEMS) Sensors for the Commercial Technology Insertion Program (CTIP)," U.S. Army Research Laboratory, Aberdeen Proving Ground, MD, ARL-MR-384, January 1998.

Davis, B.S., T.G. Brown, J.A. Condon, D. Hepner, and S. Myers, "Development of an IMU/Telemetry System for Range Flight Testing of Missiles and Rockets," 18th International Ballistics Symposium, San Antonio, TX, October 1999.

Harkins, T., "Assessing the Feasibility of Accelerometer-Only Inertial Measurement Units," U.S. Army Research Laboratory, Aberdeen Proving Ground, MD, ARL-MR-200, November 1994.

Harkins, T., B.S. Davis, and D. Hepner, "Novel On-Board Sensor Systems for Making Angular Measurements on Spinning Projectiles," SPIE AeroSense Symposium, 4365-25, Orlando, FL, April 2001.

Hathaway, A., W. Hathaway, R. Whyte, B. Davis, T. Brown, D. Hepner, and T. Harkins, "Combining Radar, Yawsonde, and On-board Telemetry Data to Determine Aerodynamic Coefficients" 51st Aeroballistic Range Association, Madrid Spain, September 2000.

Hepner, D., and T. Harkins, "Determining Inertial Orientation of a Spinning Body With Body-Fixed Sensors," U.S. Army Research Laboratory, Aberdeen Proving Ground, MD, ARL-TR-2313, January 2001.

Hepner, D., M.S.L. Hollis, and C. Mitchell, "Yawsonde Technology for the Jet Propulsion Laboratory (JPL) Free-Flying Magnetometer (FFM) Program," U.S. Army Research Laboratory Technical Report, ARL-TR-1610, July 1998.

Minor, R., and D. Rowe, "Utilization of GPS/MEMS-IMU for Measurement of Dynamics for Range Testing of Missiles and Rockets," IEEE Position, Location, Navigation Symposium, pp 602-607, Palm Springs, CA, April 1998.

Whyte, R., R. Houghton, and W. Hathaway, "Description of Yawsonde Numerical Integration Data Reduction Computer Programs," U.S. Army Ballistics Research Laboratory, Aberdeen Proving Ground, MD, BRL-CR-280, May 1973.

APPENDIX A

MECHANICAL DRAWINGS

INTENTIONALLY LEFT BLANK

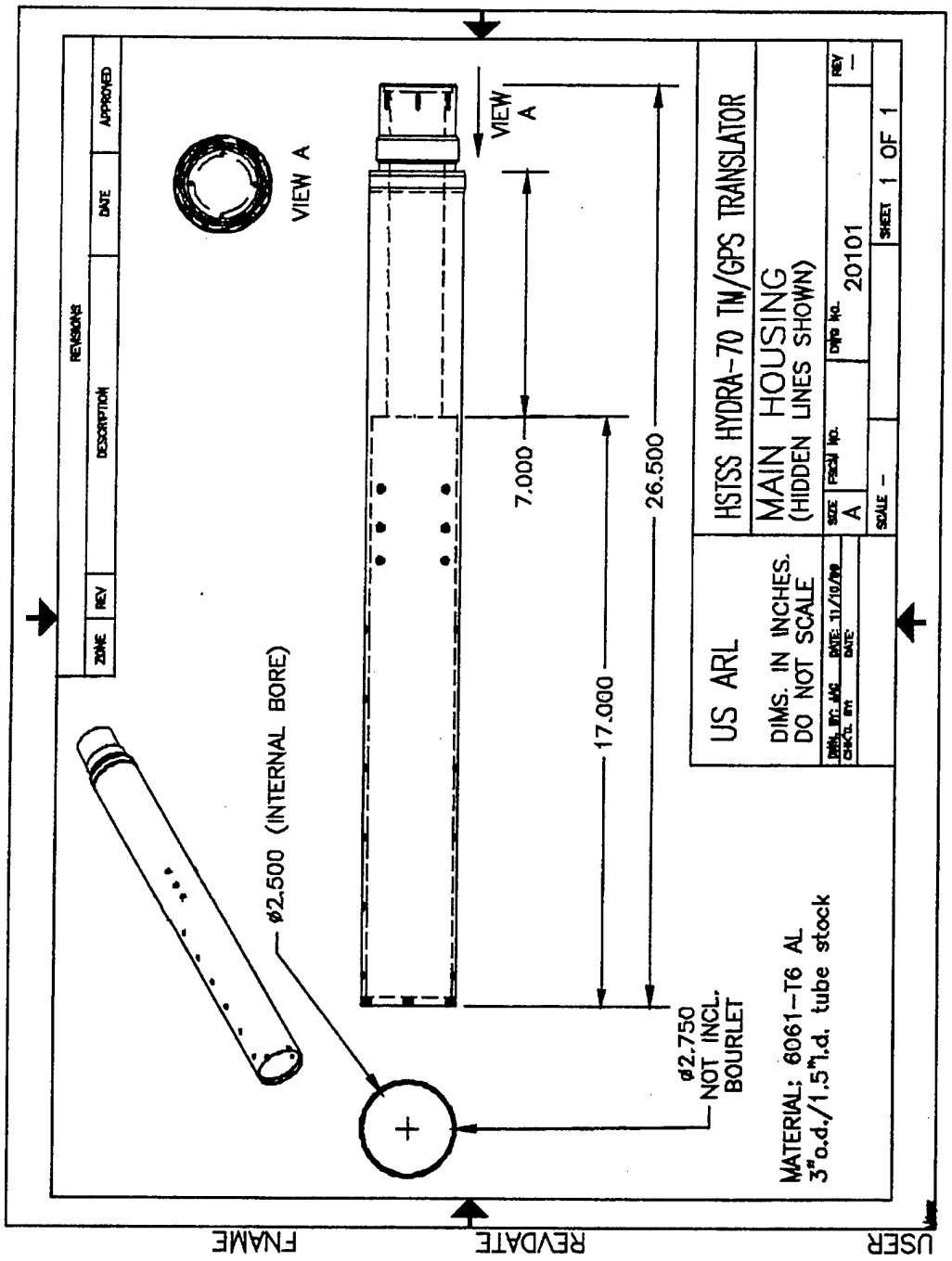

Figure A-1. Main Housing Drawing.

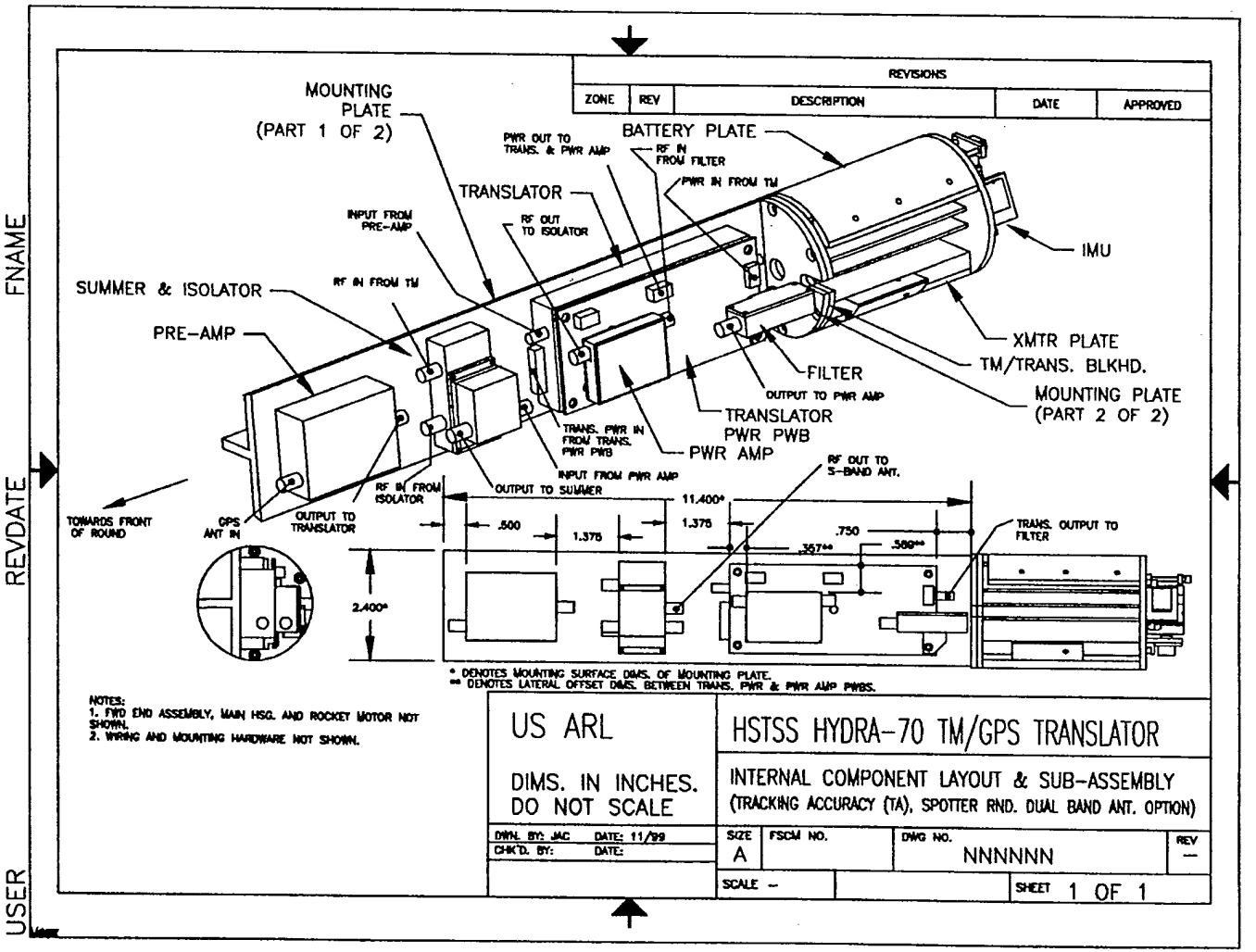

Figure A-2. Main Housing Internal Components Sub-assembly Drawing.

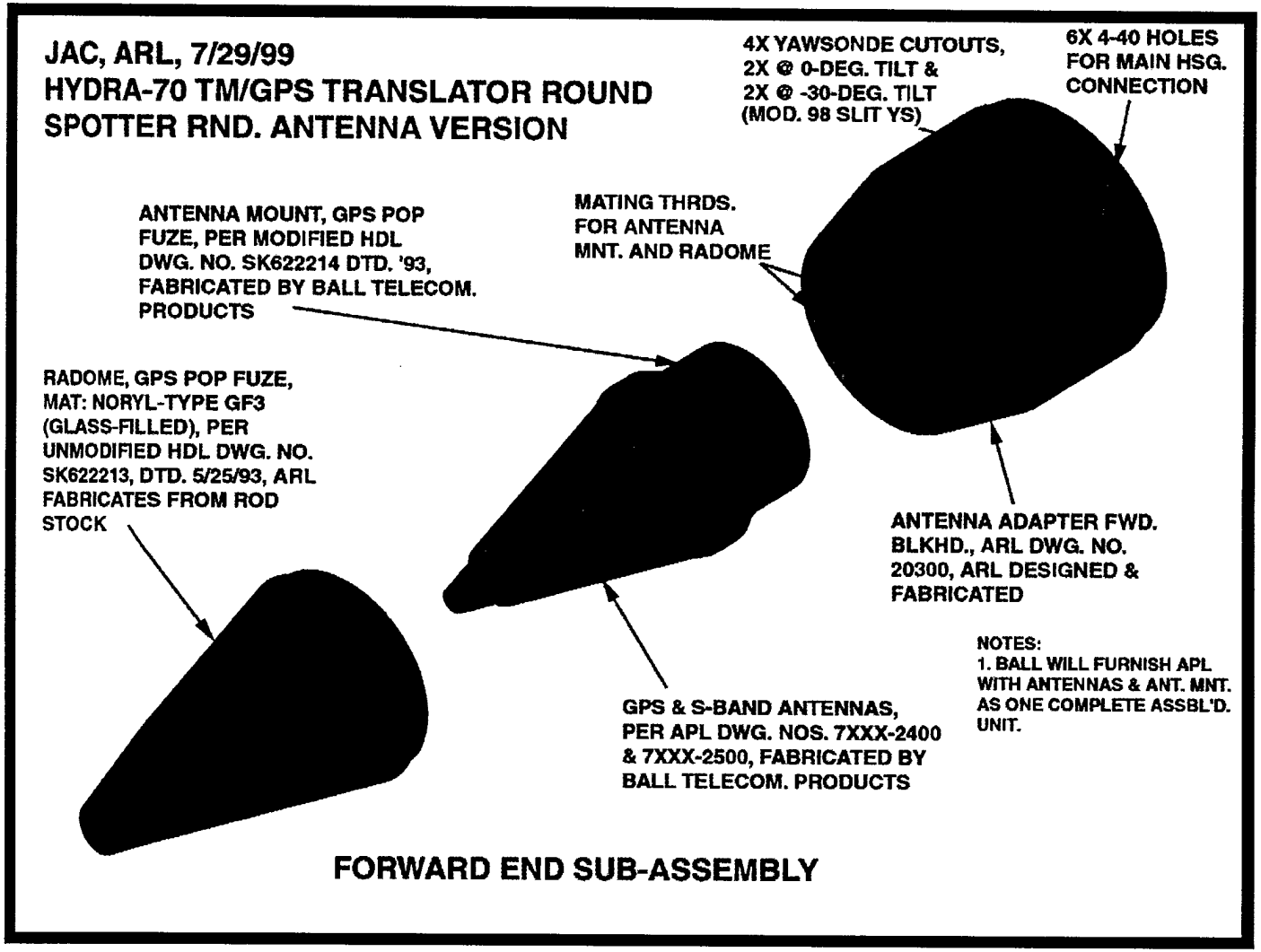

Figure A-3. Antenna Adapter Forward Bulkhead Sub-assembly..

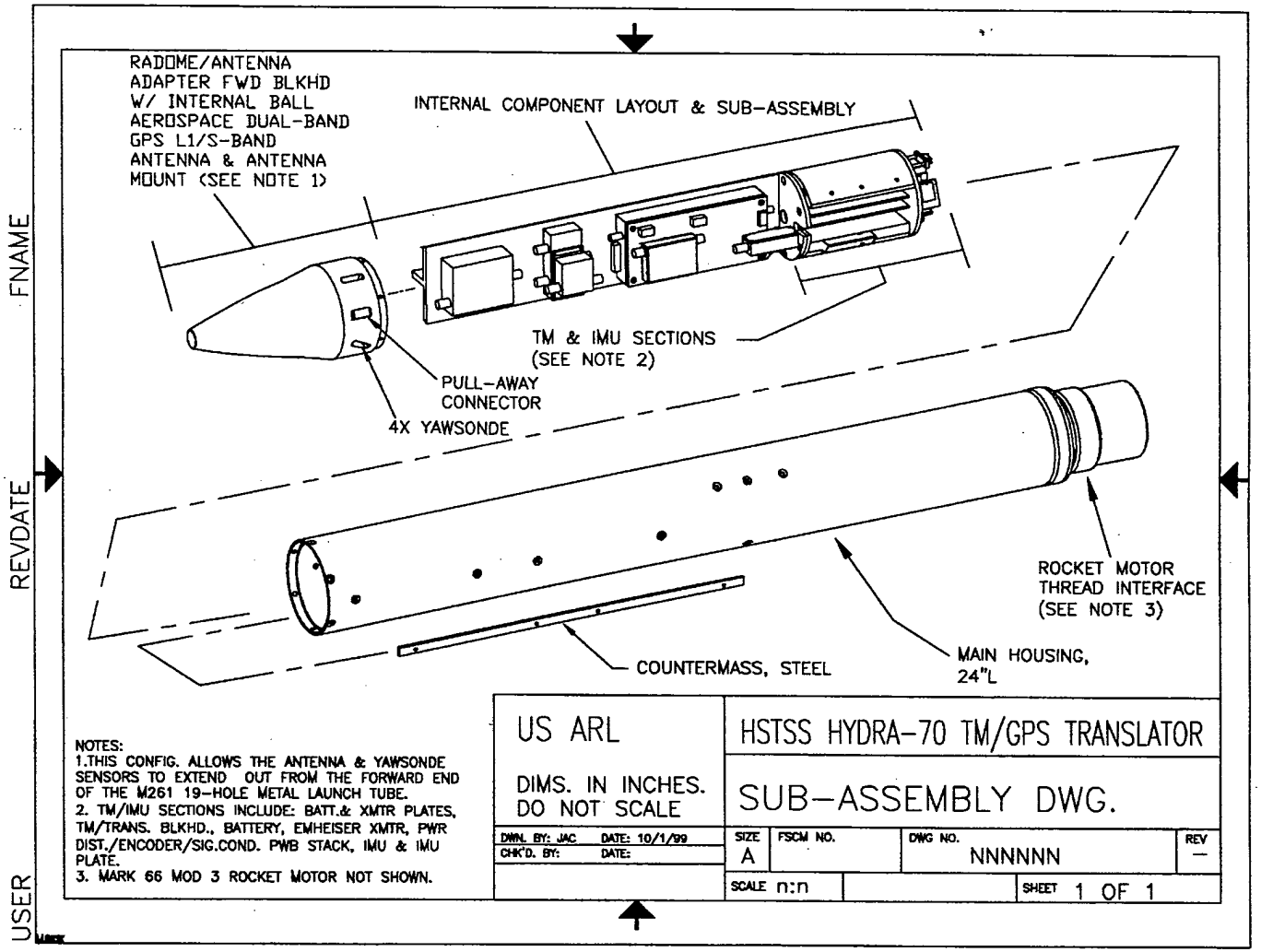

Figure A-4. Warhead Instrumentation Assembly Drawing.

APPENDIX B

FINITE ELEMENT ANALYTICAL RESULTS

INTENTIONALLY LEFT BLANK

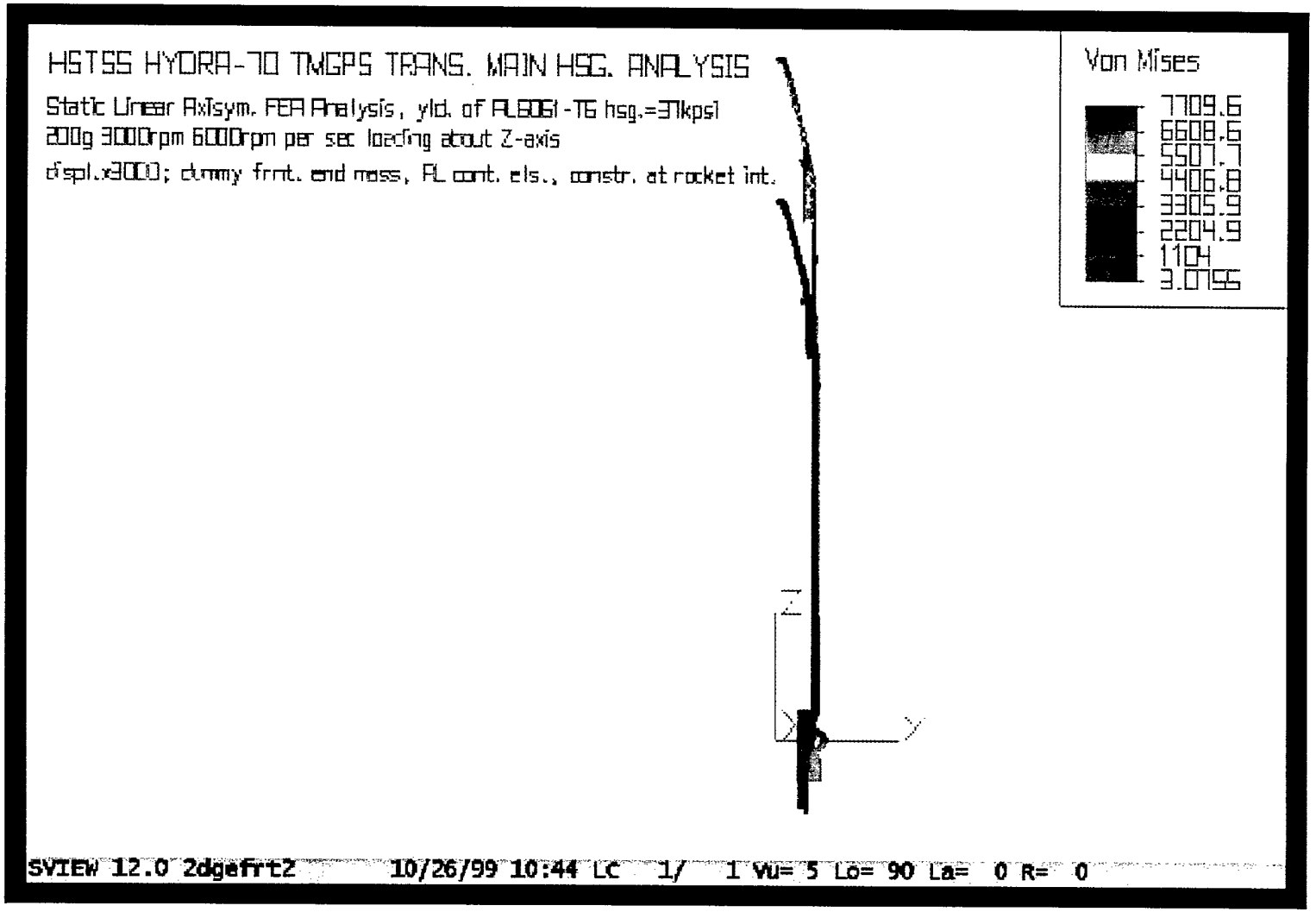

Figure B-1. Warhead Housing FEA Results (full model shown).

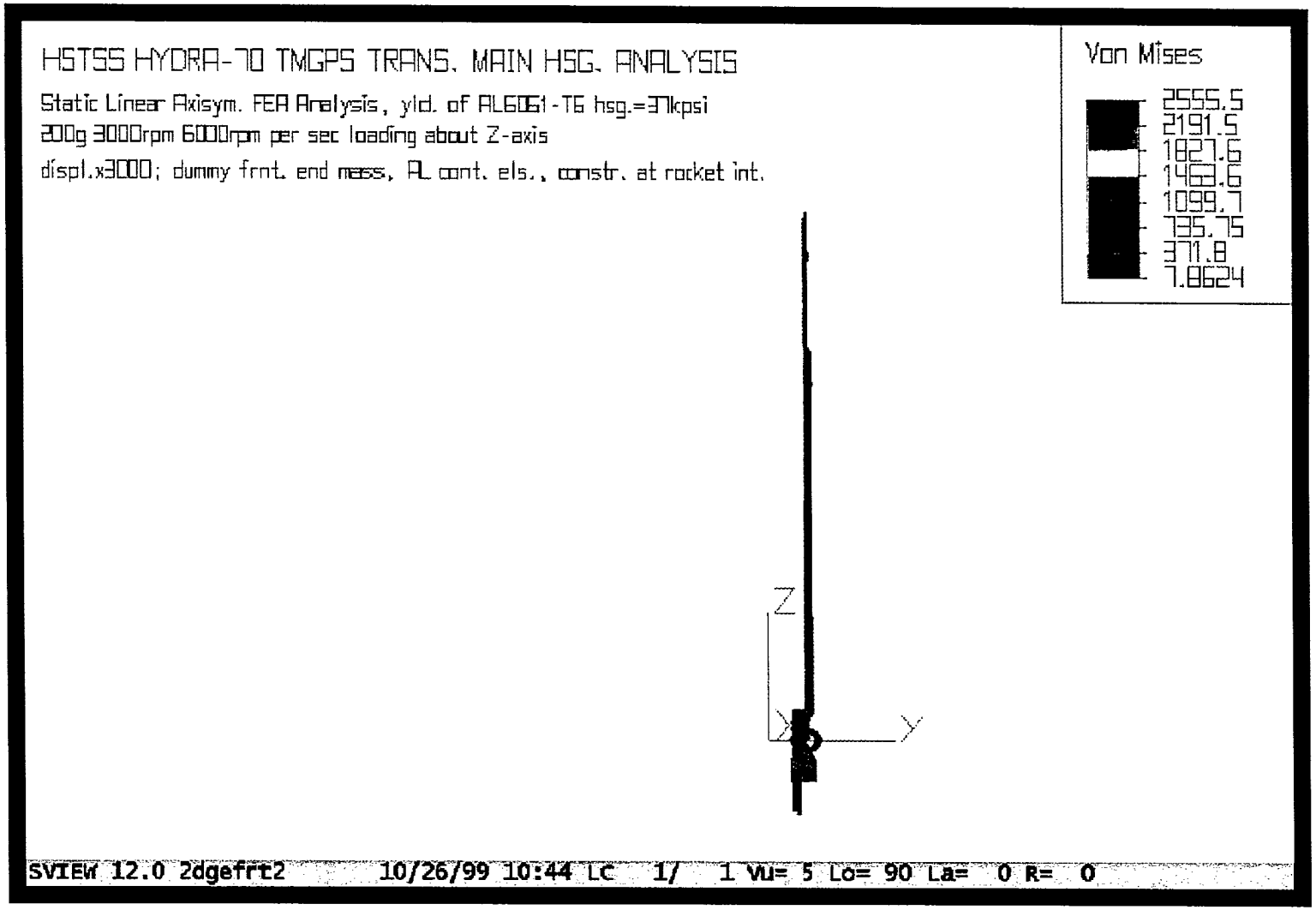

Figure B-2. Warhead Housing FEA Results (only housing shown).

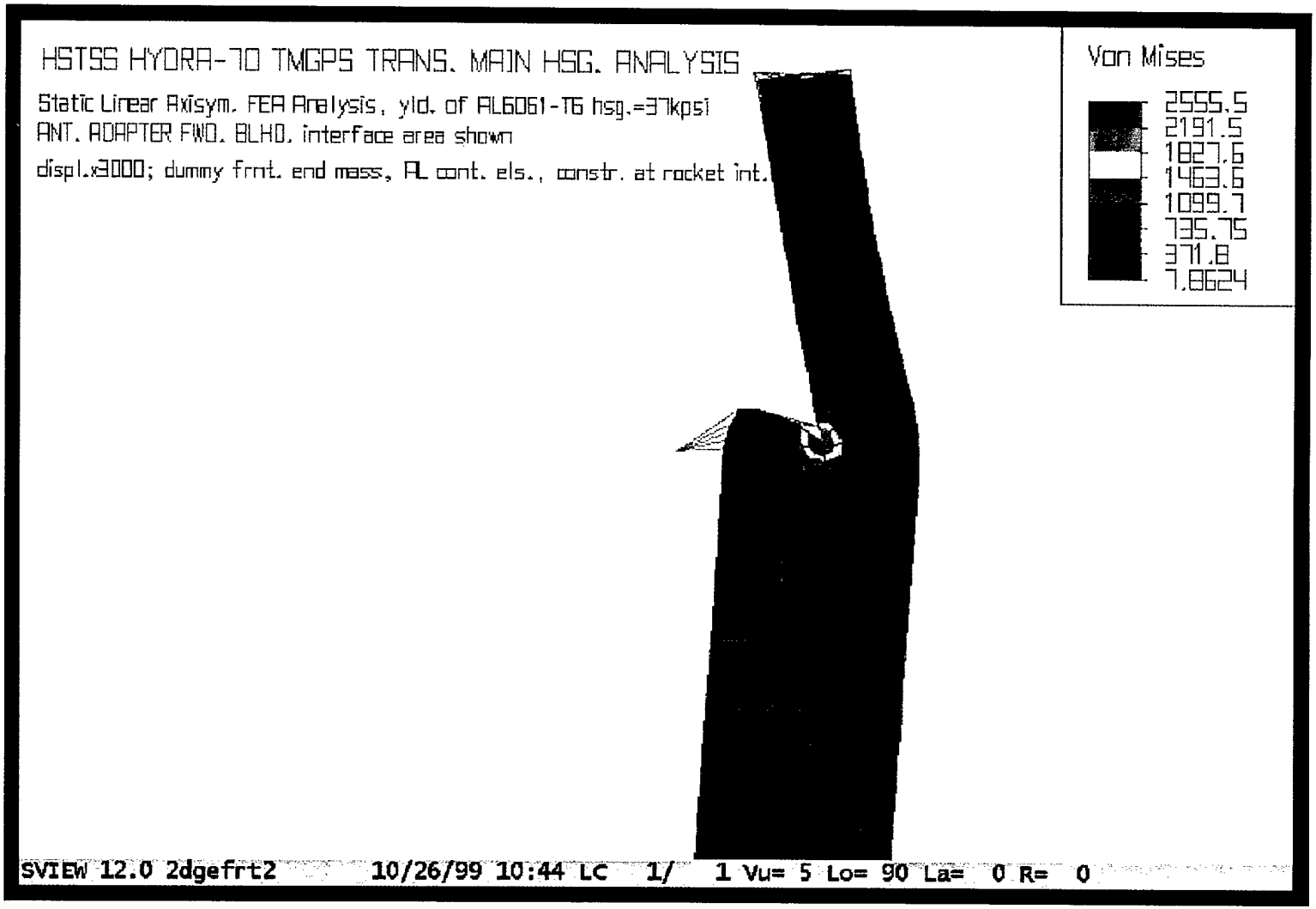

Figure B-3. Warhead Housing FEA Results (zoom view of AAFB interface, top end of housing).

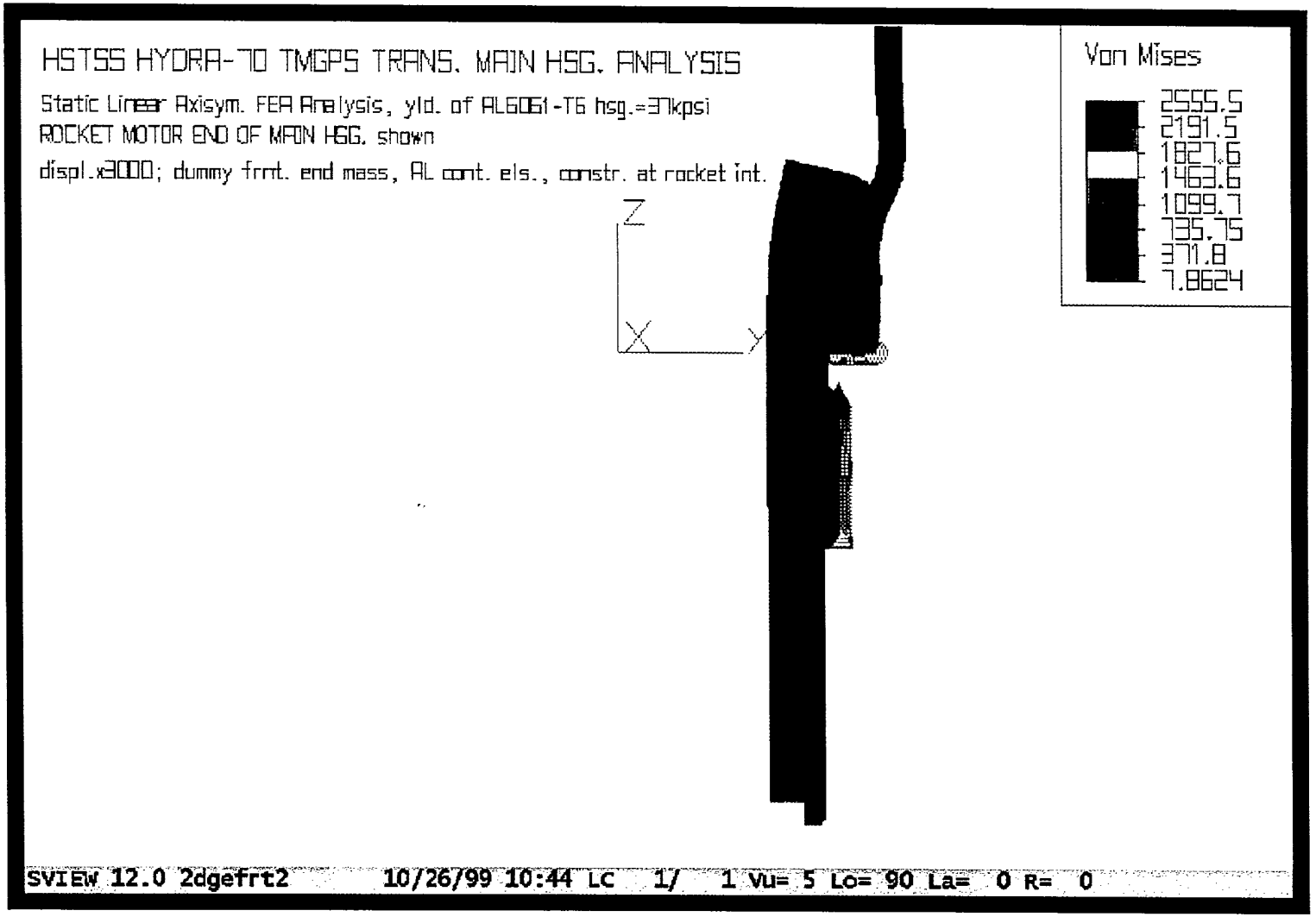

Figure B-4. Warhead Housing FEA Results (bottom end of housing).

APPENDIX C

PRODAS 2000 PRELIMINARY AERODYNAMICS MODEL

INTENTIONALLY LEFT BLANK

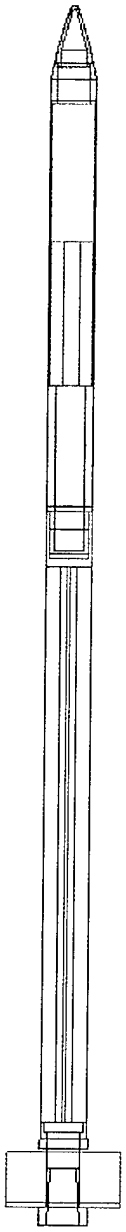

Figure C-1. PRODAS 2000 Warhead Instrumentation System Model.

Table C-1. Aerodynamic Coefficients of Warhead Instrumentation System Model

Mach	CXO	CX2	CNa	CPN	CXfore	CXbase	CNq	Cma	Cmq	Clp	Cld
0.010	0.380	7.3	8.8	17.4	0.235	0.145	293	-44.2	-2906	-11	0.035
0.400	0.381	7.3	9.3	17.8	0.229	0.152	317	-49.9	-3040	-11	0.035
0.600	0.381	7.3	9.5	17.9	0.226	0.155	329	-52.9	-3109	-11	0.035
0.700	0.392	7.5	9.9	18.1	0.232	0.160	345	-56.7	-3201	-11	0.035
0.750	0.397	7.7	10.1	18.2	0.235	0.162	353	-58.6	-3246	-11	0.035
0.800	0.402	7.8	10.2	18.3	0.238	0.165	361	-60.5	-3292	-11	0.035
0.850	0.431	8.0	10.6	18.4	0.264	0.167	375	-63.3	-3358	-11	0.035
0.875	0.445	8.1	10.8	18.4	0.278	0.168	382	-64.7	-3391	-11	0.035
0.900	0.460	8.2	11.0	18.4	0.291	0.169	389	-66.1	-3424	-11	0.035
0.925	0.494	8.4	11.1	18.4	0.324	0.170	396	-67.4	-3450	-11	0.035
0.950	0.528	8.6	11.3	18.5	0.356	0.171	403	-68.8	-3477	-11	0.035
0.975	0.587	9.4	11.5	18.5	0.395	0.193	409	-70.1	-3504	-11	0.035
1.000	0.647	10.2	11.7	18.5	0.433	0.214	416	-71.4	-3531	-11	0.035
1.025	0.685	11.0	11.8	18.7	0.472	0.213	426	-74.2	-3596	-11	0.035
1.050	0.723	11.8	11.9	18.8	0.511	0.211	435	-76.9	-3662	-11	0.035
1.100	0.714	13.4	12.2	19.1	0.503	0.211	454	-81.3	-3833	-11	0.032
1.200	0.700	16.1	11.6	18.7	0.493	0.207	426	-73.7	-3701	-11	0.003
1.350	0.678	15.5	11.0	18.2	0.477	0.201	390	-63.9	-3539	-12	-0.001
1.500	0.657	14.9	10.5	17.7	0.463	0.194	364	-56.4	-3449	-12	-0.001
1.750	0.624	14.3	10.4	17.4	0.443	0.181	354	-52.5	-3425	-12	0.002
2.000	0.598	13.7	8.6	15.6	0.431	0.166	258	-27.6	-2886	-12	0.020
2.250	0.573	13.4	8.1	14.8	0.421	0.152	230	-20.0	-2737	-12	0.020
2.500	0.548	13.1	7.6	14.0	0.411	0.137	202	-12.4	-2588	-12	0.020
3.000	0.510	11.5	6.9	12.8	0.398	0.111	166	-2.7	-2371	-12	0.020
3.500	0.489	10.7	6.4	11.9	0.397	0.092	141	3.2	-2198	-12	0.019
4.000	0.469	10.0	5.8	10.8	0.396	0.073	115	9.1	-2025	-11	0.016
4.500	0.457	9.2	5.5	10.2	0.395	0.062	101	12.0	-1912	-11	0.014
5.000	0.445	8.4	5.2	9.5	0.394	0.051	88	14.9	-1798	-11	0.005

Table C-2. Aerodynamic Coefficients of Warhead Instrumentation System Model

Mach	CYga	Clga	Cnga	Csm	Czd	Cmd	Cxbody	Cxfin	CNaB	CPNB	CNaFl	CPNFl
0.010	15.0	0.7	-181	13	0.15	-0.8	0.339	0.041	2.8	2.6	6.0	24.4
0.400	16.2	0.7	-195	13	0.16	-0.9	0.339	0.042	2.8	2.6	6.5	24.4
0.600	16.9	0.8	-203	13	0.17	-0.9	0.339	0.042	2.8	2.6	6.7	24.4
0.700	17.7	0.8	-213	13	0.17	-1.0	0.342	0.050	2.8	2.6	7.1	24.4
0.750	18.2	0.8	-218	13	0.18	-1.0	0.344	0.053	2.8	2.6	7.2	24.4
0.800	18.6	0.8	-223	13	0.18	-1.1	0.345	0.057	2.8	2.6	7.4	24.4
0.850	19.4	0.9	-231	16	0.18	-1.1	0.366	0.065	2.9	2.5	7.7	24.3
0.875	19.8	0.9	-235	19	0.19	-1.1	0.376	0.069	2.9	2.5	7.9	24.3
0.900	20.2	0.9	-240	43	0.19	-1.2	0.387	0.073	2.9	2.5	8.0	24.3
0.925	20.6	0.9	-244	48	0.19	-1.2	0.418	0.076	3.0	2.4	8.2	24.2
0.950	21.0	1.0	-248	49	0.20	-1.2	0.450	0.078	3.0	2.4	8.3	24.2
0.975	21.4	1.0	-252	51	0.20	-1.2	0.507	0.081	3.0	2.4	8.5	24.2
1.000	21.8	1.0	-257	45	0.20	-1.3	0.563	0.083	3.0	2.4	8.7	24.2
1.025	22.1	1.0	-262	20	0.21	-1.3	0.601	0.084	3.0	2.5	8.8	24.3
1.050	22.4	1.0	-268	0	0.21	-1.3	0.638	0.084	3.0	2.6	8.9	24.4
1.100	23.0	1.0	-280	0	0.21	-1.4	0.635	0.078	3.1	2.6	9.1	24.6
1.200	21.4	1.0	-263	0	0.20	-1.3	0.630	0.071	3.1	2.5	8.5	24.6
1.350	19.5	0.9	-241	0	0.19	-1.1	0.612	0.066	3.2	2.5	7.8	24.7
1.500	18.2	0.8	-225	0	0.18	-1.0	0.594	0.062	3.3	2.4	7.2	24.7
1.750	17.7	0.8	-218	0	0.18	-0.9	0.567	0.057	3.4	2.4	7.0	24.7
2.000	12.9	0.6	-159	0	0.15	-0.5	0.543	0.055	3.5	2.3	5.1	24.7
2.250	11.5	0.5	-142	0	0.14	-0.4	0.520	0.053	3.6	2.2	4.6	24.7
2.500	10.1	0.5	-125	0	0.13	-0.2	0.498	0.050	3.6	2.1	4.0	24.7
3.000	8.3	0.4	-102	0	0.12	-0.1	0.463	0.047	3.6	1.8	3.3	24.7
3.500	7.0	0.3	-87	0	0.11	0.1	0.444	0.046	3.6	1.8	2.8	24.7
4.000	5.8	0.3	-71	0	0.10	0.2	0.425	0.044	3.5	1.8	2.3	24.7
4.500	5.1	0.2	-63	0	0.10	0.2	0.414	0.043	3.5	1.8	2.0	24.7
5.000	4.4	0.2	-54	0	0.09	0.3	0.403	0.042	3.4	1.8	1.7	24.7

INTENTIONALLY LEFT BLANK

APPENDIX D

EXPERIMENTAL DATA REQUIREMENTS LIST

INTENTIONALLY LEFT BLANK

EXPERIMENTAL DATA REQUIREMENTS LIST

The following is a complete list of measurements required for input into Arrow Tech's TRYDAS Program.

1. Projectile Physical Data
   - Reference Diameter, m
   - Projectile Weight, kg
   - Axial Inertia, kg-m^2
   - Transverse Inertia, kg-m^2

2. Test Setup, Weapon, and Firing Data
   - Test Site Location (Yuma PG, Dugway PG, Aberdeen PG, etc.)
   - Test Date and Time of Firing
   - Quadrant Elevation, Gunners mils
   - Azimuth of Fire, degrees from North (firing east is +90 degrees)
   - Gun Coordinates, x_g, y_g, z_g, m (x-East y-North z-Up)
   - Radar Coordinates, x_r, y_r, z_r, m (x-East y-North z-Up)
   - Impact Altitude, z_{fine}, m
   - First Max Yaw (estimate), degrees
   - Muzzle Velocity (estimate), m/s
   - Muzzle Exit Twist (Spinner), calibers/turn
   - or Muzzle Spin (Finner), radians/sec
   - Motor or Base Bleed On Time, s
   - Motor or Base Bleed Off Time, s

3. Met File Table (Gun Altitude to Apogee)
   - Altitude, m
   - Pressure, mbars
   - Temperature, deg-C
   - Wind Direction, degrees from North
   - Wind Speed, m/sec

4. Solarsonde File
   - Time, seconds
   - Spin Rate, cycles/sec
   - Sun Angle Compliment, degrees (90 - True Sigma; i.e. ARL)

5. Tracking Radar File
   - Time, seconds
   - Radial Velocity, m/s
   - Azimuth, deg
   - Elevation, deg
   - Signal-To-Noise Ratio, (leave blank if not available)

6. The estimated coefficients as functions of Mach number (pr2 file)
   - Axial Force Coefficient
   - Yaw Axial Force Coefficient Derivative
   - Normal Force Coefficient Derivative
   - Pitching Moment Coefficient Derivative
   - Pitch Damping Moment Coefficient
   - Magnus Moment Coefficient Derivative at zero yaw
   - Cubic Magnus Moment Coefficient Derivative (required for Spinners)
   - Quintic Magnus Moment Coefficient Derivative (required for Spinners)
   - Roll Damping Moment Coefficient
   - Roll Moment Coefficient (required for Finners)
   - The analysis code also accepts a Rocket Thrust table as an optional user input. The use of this table is suggested for tests involving the 155mm M549, 155mm M982, HYDRA-70 rockets or other rocket assisted projectiles.

7. IMU sensor data (accelerometers, magnetometers, and rate sensors)
   - Physical location of the sensors
   - Time, seconds
   - Acceleration, Magnetic Angle, Rate, etc. data in engineering units

8. GPS data
   - Physical location of the antenna
   - Time, X, Y, Z, Vx, Vy, Vz data in engineering units

NO. OF COPIES	ORGANIZATION
1	ADMINISTRATOR DEFENSE TECHNICAL INFO CTR ATTN DTIC OCA 8725 JOHN J KINGMAN RD STE 0944 FT BELVOIR VA 22060-6218
1	DIRECTOR US ARMY RSCH LABORATORY ATTN AMSRL CI AI R REC MGMT 2800 POWDER MILL RD ADELPHI MD 20783-1197
1	DIRECTOR US ARMY RSCH LABORATORY ATTN AMSRL CI LL TECH LIB 2800 POWDER MILL RD ADELPHI MD 20783-1197
1	DIRECTOR US ARMY RSCH LABORATORY ATTN AMSRL D D SMITH 2800 POWDER MILL RD ADELPHI MD 20783-1197
1	DIRECTOR US ARMY RSCH LABORATORY ATTN AMSRL WM MB A FRYDMAN 2800 POWDER MILL RD ADELPHI MD 20783-1197
9	DIRECTOR US ARMY RSCH LABORATORY ATTN AMSRL SE RL T OLDHAM M DUBEY B PIEKARSKI AMSRL SE S J EIKE AMSRL SE SA J PRICE AMSRL SE SS LADAS A EDELSTEIN D FLIPPEN AMSRL SE EE Z SZTANKAY 2800 POWDER MILL RD ADELPHI MD 20783-1197
4	COMMANDER US ARMY TACOM ARDEC ATTN AMSTA AR CCF A C ROBINSON M D'ONOFRIO W KONICK B CHRISTOPHERSON 2800 POWDER MILL RD ADELPHI MD 20783-1197

NO. OF COPIES	ORGANIZATION
1	US ARMY CECOM ATTN J VIG FORT MONMOUTH NJ 07703-5203
1	CDR US ARMY TACOM ARDEC ATTN AMSTA AR QAC M BOMUS PICATINNY ARSENAL NJ 07806-5000
3	CDR US ARMY TACOM ARDEC ATTN AMSTA AR FSF T S CHUNG M AMORUSO AMSTA AR FSF D C PEREIRA PICATINNY ARSENAL NJ 07806-5000
4	CDR US ARMY TACOM ARDEC ATTN AMSTA AR CCH B G EUSTICE F CHANG R SAYER F RENNER PICATINNY ARSENAL NJ 07806-5000
6	CDR US ARMY TACOM ARDEC ATTN AMSTA AR FSP S PEARCY AMSTA AR FSP G S DEFEO P GRANGER D CARLUCCI R WERKO AMSTA AR FSP E A BAHIA PICATINNY ARSENAL NJ 07806-5000
2	CDR US ARMY TACOM ARDEC ATTN AMSTA AR FS A WARNASCH AMSTA AR FSA K CHIEFA PICATINNY ARSENAL NJ 07806-5000
5	CDR US ARMY TACOM ARDEC ATTN AMSTA AR CCH A R CARR M LUCIANO G KOLASA M PALATHINGAL D VO PICATINNY ARSENAL NJ 07806-5000
2	CDR US ARMY TACOM ARDEC ATTN AMSTA AR CCL B R MAZESKI D AHMAD PICATINNY ARSENAL NJ 07806-5000
1	CDR US ARMY TACOM ARDEC ATTN AMSTA AR RMP N GRAY PICATINNY ARSENAL NJ 07806-5000
1	CDR US ARMY TACOM ARDEC ATTN AMSTA AR CCL A E REMFER PICATINNY ARSENAL NJ 07806-5000

NO. OF COPIES ORGANIZATION

1 CDR US ARMY TACOM ARDEC
ATTN SFAE GCSS BM
R KOWALSKI
PICATINNY ARSENAL NJ 07806-5000

1 CDR US ARMY TACOM ARDEC
ATTN SFAE GCSS ARMS
C GRASSANO
PICATINNY ARSENAL NJ 07806-5000

1 DARPA/MTO
ATTN W TANG
3701 N FAIRFAX DRIVE
ARLINGTON VA 22203-1714

7 CDR NAVAL SURF WARFARE CTR
ATTN G33 J FRAYSSE G32 ELLIS
G34 H WENDT G61 LARACH
D HAGEN A EVANS
B52 M ABAIE
17320 DAHLGREN ROAD
DAHLGREN VA 22448-5100

8 CDR NAVAL SURF WARFARE CTR
INDIAN HEAD DIVISION
ATTN CODE 40D D GARVICK
CODE 4110C L FAN
CODE 4110C K JOHNSON
CODE 4120 V CARLSON
CODE 440C4 P SMITH
CODE 450D T GRIFFIN
CODE 5710 E EAGLES
CODE 57 C PARAS
101 STRAUSS AVE
INDIAN HEAD MD 20640-5035

1 CDR NAVAL SURF WARFARE CTR
DAHLGREN DIVISION
ATTN CODE 40D J BLANKENSHIP
6703 WEST HIGHWAY 98
PANAMA CITY FL 32407-7001

1 IDA
SCIENCE AND TECH DIV
ATTN H LAST
1801 N BEAUREGARD ST
ALEXANDRIA VA 22311-1772

2 CDR OFC OF NAVAL RSCH
ATTN CODE 333 P MORRISSON
J GOLDWASSER
800 N QUINCY ST RM 507
ARLINGTON VA 22217-5660

NO. OF COPIES ORGANIZATION

2 CDR AFRL/MNMF
ATTN S ROBERSON R MABRY
306 W EGLIN BLVD STE 219
EGLIN AFB FL 32542-6810

2 CDR NAWC WEAPONS DIV
ATTN G BORGEN D POWELL
CODE 543200E BLDG 311
POINT MUGU CA 93042-5000

4 CDR NAVAL AIR WARFARE CTR
WEAPONS DIVISION
ATTN CODE C3923 S GATTIS
CODE C3904 D SCOFIELD
S MEYERS L ROLLINGSON
CHINA LAKE CA 93555-6100

3 PROGRAM MGR ITTS
STRICOM
ATTN AMFTI EL D SCHNEIDER
R COLANGELO
R LONGENBACH
12350 RESEARCH PKWY
ORLANDO FL 32826-3276

10 CDR US ARMY AMCOM
ATTN AMSAM RD MG NC P RUFFIN
J BAEDER V LEFEVRE
AMSAM RD MG IP
G HUTCHESON
AMSAM RD WS DP TD
S BURGETT C LEWIS
C ROBERTS B ROBERTSON
AMSAM RD WS ID P ASHLEY
T HUDSON
REDSTONE ARSENAL AL 35898-5247

1 DIRECTOR
US ARMY RTTC
ATTN STERT TE F TD R EPPS
REDSTONE ARSENAL AL 35898-8052

1 CDR US ARMY YUMA PROVING GROUND
ATTN STEYP MT AT A A HOOPER
YPG AZ 85365-9110

1 TEST ARTICLE PREP DEP
NAWCAD CODE 540000A R FAULSTICH
BLDG 1492 UNIT 1
PATUXENT MD 20670-1456

NO. OF COPIES ORGANIZATION

3 CDR US ARMY
ATTN STEYP TD ATO
A HART C RAMSDELL
D WEINGARTEN
YPG AZ 85365-9106

3 ARROW TECH ASSOCIATES
ATTN W HATHAWAY
J WHYTE R WHYTE
SOUTH BURLINGTON VT 05403

1 ALLIANT DEFENSE
ATTN A GAUZENS
PO BOX 4648
CLEARWATER FL 33758-4648

1 LOCKHEED-MARTIN-SANDERS
ATTN M CARLSON
NCA1-2078 95 CANAL ST
NASHUA NH 03061-0868

2 ALLIANT TECHSYSTEMS
ATTN C CANDLAND R DOHRN
600 SECOND ST NE
HOPKINS MN 55343-8384

2 SAIC
ATTN J DISHON G PHILLIPS
16701 W BERNARDO DR
SAN DIEGO CA 92127

1 SAIC
ATTN J GLISH
3800 W 80TH ST STE 1090
BLOOMINGTON MN 55431

1 SAIC
ATTN M PALMER
1410 SPRING HILL RD STE 400
MCLEAN VA 22102

1 SYSTEMS PLANNING CORP
ATTN M MOSES
1429 QUINCY ST
ARLINGTON VA 22207

2 ROCKWELL COLLINS
ATTN M JOHNSON R MINOR
350 COLLINS RD NE
CEDAR RAPIDS IA 52498

NO. OF COPIES ORGANIZATION

1 SWALES AEROSPACE
ATTN Q LAM
5050 POWDER MILL RD
BELTSVILLE MD 20705

1 UCLA
ATTN J JUDY
68 –121 ENGINEERING IV
BOX 951594
LOS ANGELES CA 90095-1594

7 JOHNS HOPKINS UNIV
APPLIED PHYSICS LAB
ATTN B D'AMICO M BOEHME
W DEVEREUX D WICKENDEN
R BENSON M ASHER
L LINSTROM
1110 JOHNS HOPKINS RD
LAUREL MD 20723-6099

1 UC BERKELEY
ATTN A PISANO
DEPT OF MECH ENG
5101-B ETCHEVERRY HALL
BERKELEY CA 94720-1740

9 CHLS STARK DRAPER LAB
ATTN J CONNELLY J SITOMER
R POLUTCHKO J ELWELL
A KOUREPENIS F HARRISON
D GUSTAFSON M MCCONLEY
T EASTERLY
555 TECHNOLOGY SQUARE
CAMBRIDGE MA 02139-3563

1 SUNY
ATTN R MARCHAND
DEPT OF MATH & COMPUTER SCI
FREDONIA NY 14063

3 GEORGIA TECH RSCH INST
COBB CO RSCH FACILITY
ATTN J MCMICHAEL A LOVAS
D PAREKH
7220 RICHARDSON RD
SMYRNA GA 30080

1 GEORGIA INST OF TECH
SCHOOL OF AEROSPACE ENG
ATTN A CALISE
270 FERST DR
ATLANTA GA 30332-0150

NO. OF COPIES ORGANIZATION

1 ANALOG DEVICES
ATTN T JUNEAU
2140 SHATTUCK AVE STE 205
BERKELEY CA 94704

2 ANALOG DEVICES
ATTN B SULOFF S LEWIS
21 OSBORN ST
CAMBRIDGE MA 02139-3556

1 ANALOG DEVICES
ATTN R MEISENHELDER
804 WOBURN ST
WILMINGTON MA 01887-3462

1 FIBERSENSE TECHNOLOGY CORP
ATTN C REYNOLDS
198 VANDERBILT AVE
NORWOOD MA 02062

1 HONEYWELL
ATTN MN14-3B35 M CARUSO
12001 STATE HIGHWAY 55
PLYMOUTH MN 55441

1 AEROVIRONMENT
ATTN C MIRALLES
4685-3H INDUSTRIAL ST
SIMI VALLEY CA 93063

1 ROCKWELL SCIENCE CTR
ATTN I GOLDBERG
PO BOX 1085
THOUSAND OAKS CA 91358

ABERDEEN PROVING GROUND

2 DIRECTOR
US ARMY RSCH LABORATORY
ATTN AMSRL CI LP (TECH LIB)
BLDG 305 APG AA

4 CDR US ARMAMENT RD&E CENTER
ATTN AMSTA AR FST T R LIESKE
J WHITESIDE J MATTS
F MIRABELLE
BLDG 120

1 CDR USA DTC
ATTN CSTE DTC TTM J SCHNELL
RYAN BLDG

NO. OF COPIES ORGANIZATION

1 CDR ATC
ATTN K MCMULLEN
BLDG 359

2 DIR USARL
ATTN AMSRL WM J SMITH
T ROSENBERGER
BLDG 4600

2 DIR USARL
ATTN AMSRL WM B A HORST
W CIEPIELLA
BLDG 4600

25 DIR USARL
ATTN AMSRL WM BA
T BROSSEAU T BROWN (5 CYS)
J CONDON (5 CYS)
B DAVIS (5 CYS)
T HARKINS D HEPNER
M HOLLIS G KATULKA
D LYON R MCGEE
P MULLER P PEREGINO
A THOMPSON
BLDG 4600

12 DIR USARL
ATTN AMSRL WM BC P PLOSTINS
M BUNDY G COOPER
J GARNER B GUIDOS
K HEAVEY J NEWILL
V OSKAY J SAHU
K SOENCKSEN D WEBB
P WEINACHT J DESPIRITO
BLDG 390

5 DIR USARL
ATTN AMSRL WM BF J LACETERA
H EDGE P HILL
T HAUG J SPANGLER
BLDG 390

2 DIR USARL
ATTN AMSRL WM RP J BORNSTEIN
C SHOEMAKER
BLDG 1121

2 DIR USARL
ATTN AMSRL WM MB C HOPPEL
AMSRL WM MC R ADLER
BLDG 4600

NO. OF
COPIES ORGANIZATION

7 DIR USARL
ATTN AMSRL WM T B BURNS
AMSRL WM TB R LOTTERO
AMSRL WM TC R COATES
W DEROSSET R MUDD
AMSRL WM TD F GREGORY
N GNIAZOWSKI
BLDG 309

INTENTIONALLY LEFT BLANK

REPORT DOCUMENTATION PAGE

Form Approved OMB No. 0704-0188

1. AGENCY USE ONLY *(Leave blank)*	2. REPORT DATE	3. REPORT TYPE AND DATES COVERED
	November 2001	Final

4. TITLE AND SUBTITLE

Flight Demonstration Results of an Inertial Measurement Unit and Global Positioning System Translator Telemetry System

5. FUNDING NUMBERS

PR: 1L162618AH80

6. AUTHOR(S)

Davis, B.S.; Condon, J.A.; Brown, T.G. (all of ARL)

7. PERFORMING ORGANIZATION NAME(S) AND ADDRESS(ES)

U.S. Army Research Laboratory
Weapons & Materials Research Directorate
Aberdeen Proving Ground, MD 21005-5066

8. PERFORMING ORGANIZATION REPORT NUMBER

9. SPONSORING/MONITORING AGENCY NAME(S) AND ADDRESS(ES)

U.S. Army Research Laboratory
Weapons & Materials Research Directorate
Aberdeen Proving Ground, MD 21005-5066

10. SPONSORING/MONITORING AGENCY REPORT NUMBER

ARL-TR-2630

11. SUPPLEMENTARY NOTES

12a. DISTRIBUTION/AVAILABILITY STATEMENT

Approved for public release; distribution is unlimited.

12b. DISTRIBUTION CODE

13. ABSTRACT *(Maximum 200 words)*

The U.S. Army Research Laboratory (ARL) has been evaluating global positioning system (GPS) technology and strap-down inertial measurement units (IMUs) configured from inexpensive, miniature micro-electro-mechanical systems for the purposes of obtaining aerodynamics, trajectory reconstruction, and/or diagnostic information. A GPS translator from the Johns Hopkins University Applied Physics Laboratory and a low-cost IMU designed by ARL from commercial off-the-shelf components were combined with a telemetry system, packaged into a 2.75-inch HYDRA-70 rocket platform, and flight demonstrated. The on-board IMU sensors included accelerometers for measuring the thrust axis and lateral accelerations, angular rate sensors for measuring pitch and yaw rate, a dual axis magnetometer for roll rate and angular yawing motion, and sun-sensing optical sensors to provide a truth measurement for the rate sensor and magnetometer data. Hawk and Weibel tracking radars were also used as a truth measurement of the rocket's velocity and position for comparison to the acquired GPS data and integrated IMU accelerometer data. Results from comparisons of the IMU sensor data to the truth measurements suggest that reasonable aerodynamics and trajectory reconstruction can be achieved. The instrumentation system's development, calibration, demonstration, and the experimental results are described.

14. SUBJECT TERMS

accelerometer inertial measurement unit rocket
gyroscopes MEMS

15. NUMBER OF PAGES

75

16. PRICE CODE

17. SECURITY CLASSIFICATION OF REPORT	18. SECURITY CLASSIFICATION OF THIS PAGE	19. SECURITY CLASSIFICATION OF ABSTRACT	20. LIMITATION OF ABSTRACT
Unclassified	Unclassified	Unclassified	